RGNZ/MGPB

Identification of AVO Attribute Response to the Presence of CO_2 Content Using AVO Modelling Method in Lower Talang Akar Formation (LTAF), South Sumatra Basin

Rudarsko-geološko-naftni zbornik
(The Mining-Geology-Petroleum Engineering Bulletin)
UDC: 550.3
DOI: 10.17794/rgn.2024.3.8

Original scientific paper

Muhammad Reza Perdana[1]; Muhammad Noor Alamsyah[2,5]; Sigit Sukmono[3]; Andri Hendriyana[4]

[1]*Faculty of Mining and Petroleum Engineering, Institut Teknologi Bandung, Jalan Ganesa 10, Bandung 40132, Indonesia. https://orcid.org/0009-0009-0782-9464*

[2]*Faculty of Mining and Petroleum Engineering, Institut Teknologi Bandung, Jalan Ganesa 10, Bandung 40132, Indonesia. https://orcid.org/0000-0003-3725-3573*

[3]*Faculty of Mining and Petroleum Engineering, Institut Teknologi Bandung, Jalan Ganesa 10, Bandung 40132, Indonesia. https://orcid.org/0000-0003-1325-5937*

[4]*Faculty of Mining and Petroleum Engineering, Institut Teknologi Bandung, Jalan Ganesa 10, Bandung 40132, Indonesia. https://orcid.org/0000-0002-9003-2385*

[5]*Exploitation Department, PetroChina International Jabung Ltd., JL. HR. Rasuna Said Blok X-7 Kav. 5, Jakarta 12710, Indonesia.*

Abstract

The research area is an oil and gas field that is currently undergoing development, located in the South Sumatra Basin. Coal content, particularly within the Lower Talang Akar Formation (LTAF) interval, is frequently encountered in this field, with coal serving as the source of in-situ CO_2 content formation. Consequently, CO_2 content can be identified using the Amplitude Versus Offset (AVO) analysis method, allowing an assessment of its influence on the percentage presence of CO_2. The data used in this study consist of well data, including log data (Density, Porosity, Vp & Vs Sonic/DT), Drill Stem Test (DST) data, well marker data resulting from stratigraphic sequence interpretation, and well reports. The AVO method to be employed encompasses a wide-angle range, approximately 0°-45°. The results obtained from this research using the AVO method, after AVO modelling on well data, indicate that the dominant AVO response within the LTAF interval is class 4 AVO. AVO analysis results regarding AVO presence indicate that reservoir intervals containing CO_2 content will exhibit a class 4 AVO response, and an increase in fluid content percentage will result in a more positive intercept and a more negative gradient (towards class 2 AVO). In terms of facies and depth variations, the AVO attribute response consistently demonstrates an increase in intercept and a decrease in gradient with rising CO_2 levels.

Keywords:
Lower Talang Akar Formation; CO_2 content; AVO attribute analysis; AVO modelling; Intercept; Gradient

1. Introduction

This research focuses on the Lower Talang Akar Formation (LTAF) interval, South Sumatra Basin (see **Figure 1**). The LTAF itself formed during the late Oligocene to early Miocene, at which time the syn-rift process was in its final phase and the post-rift process began, meaning that the prevailing sedimentation type is fluvial to deltaic, with the Upper Talang Akar Formation (UTAF) serving as a quite effective hydrocarbon trap due to its marginal marine sedimentation (see **Figure 2**) (**Ginger and Fielding, 2005; Alamsyah et al., 2023**). Therefore, sand bar occurrences with high sand content are often found in the LTAF formation, indicating the presence of quite a few hydrocarbon reservoirs. Additionally, coal content is frequently encountered in this basin, where coal serves as the source of in-situ CO_2 content formation (**Ginger and Fielding, 2005; Alamsyah et al., 2023**). The Lower Talang Akar Formation (LTAF) in the South Sumatra Basin has been the subject of several studies, one of which is the seismic anisotropy estimation of the Talang Akar Formation using ultrasonic tomography in core plugs (**Sari et al., 2018**). Consequently, CO_2 content can be identified using one seismic interpretation method, namely the Amplitude Versus Offset (AVO) analysis method, and its influence on the percentage of CO_2 presence can be observed.

The Amplitude Versus Offset (AVO) analysis is a relevant method for identifying CO_2, as several studies related to Carbon Capture Storage (CCS) monitoring have been conducted in various fields. For example, research by **Dupuy et al. (2017)** in the Utsira Formation, Sleipner, focused on the use of the AVO method for CO_2 monitoring (**Dupuy et al., 2017**). The study established a relationship between elastic properties and changes in CO_2 saturation values. The application of the AVO inversion method in the Sleipner field by **Dupuy et al.**

Corresponding author: Muhammad Reza Perdana
e-mail address: muhammadrezaperdana0611@gmail.com

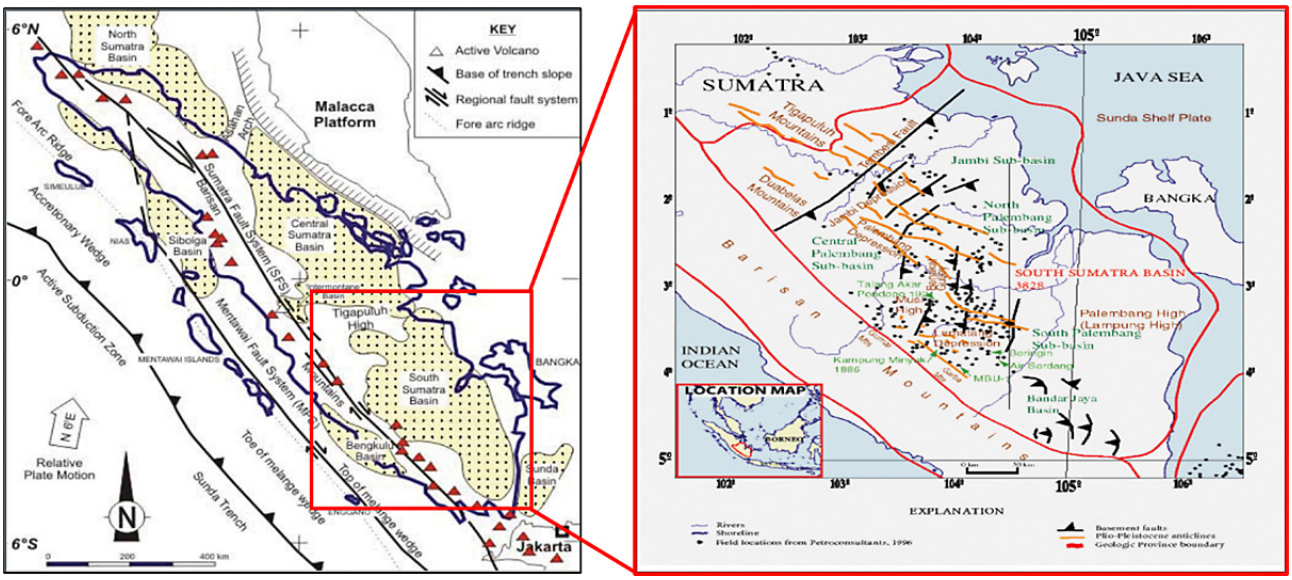

Figure 1: Research location is in the South Sumatra Basin (from **Setyaningsih et al., 2015**)

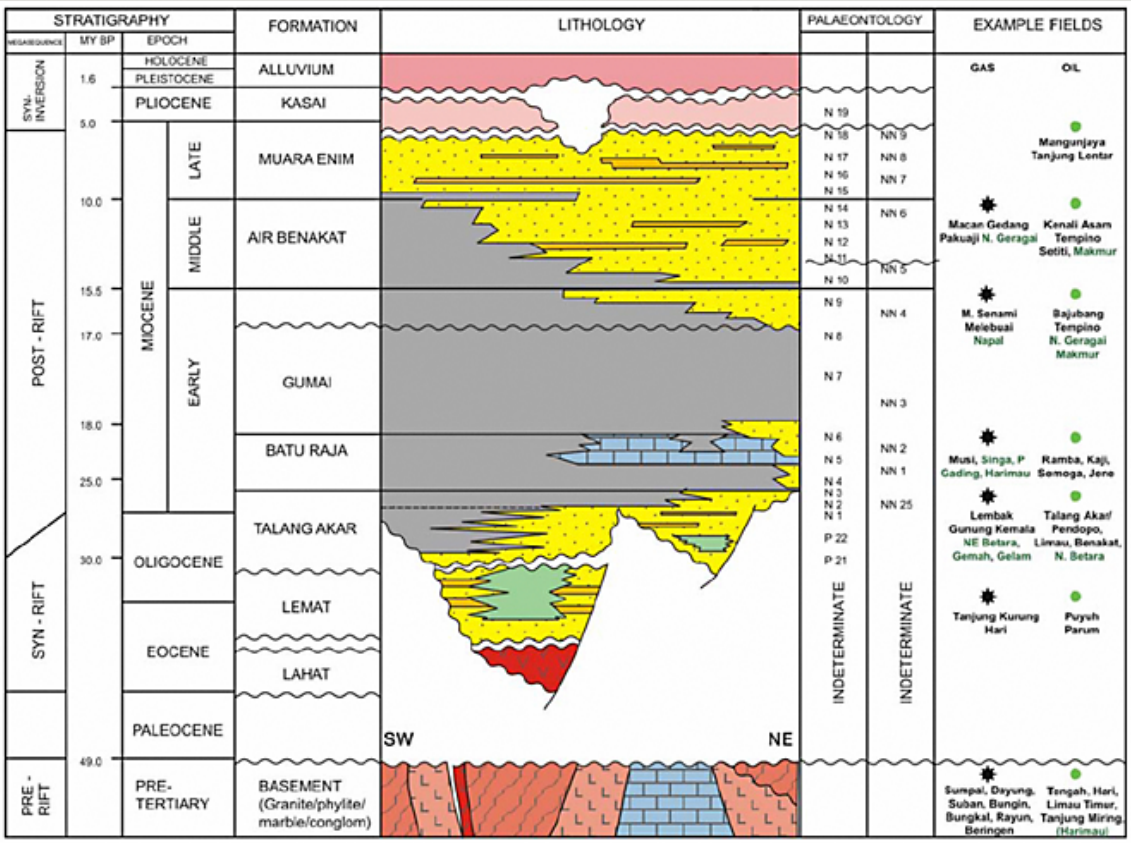

Figure 2: Chronostratigraphy of South Sumatra Basin (from **Ginger and Fielding, 2005**)

(2017) concluded that the impedance contrast produced by the AVO inversion method with Smith and Gidlow's approximation has good quality compared to the poor quality of Velocity (Vp and Vs) contrast. Another study by **Anyosa et al. (2021)** addressed CCS monitoring related to leakage due to faults, which is one of the risks of CCS (**Anyosa et al., 2021**). This research was conducted in Smeaheia, Norway, involving various simulations, including AVO modelling. Therefore, it can be said that the CO_2 effect on a reservoir will significantly alter AVO seismic responses within a specific saturation range based on these two studies.

AVO attribute analysis has undergone several developments over time, with widely used AVO approxima-

tion equations such as the **Aki and Richards (2002)** (**Equation 1**), **Wiggins et al. (1983)** (**Equation 2**), **Shuey (1985)** (**Equation 3**), and **Fatti et al. (1994)** (**Equation 4)**, as follows.

$$R_p(\theta) = a\frac{\Delta V_p}{V_p} + b\frac{\Delta\rho}{\rho} + c\frac{\Delta V_s}{V_s} \quad (1)$$

Where are:

V_p – P-wave velocity (m/s),
V_s – S-wave velocity (m/s),
ρ – density (g/cm^3).

$$R(\theta) = \frac{1}{2}\left[\frac{\Delta\alpha}{\alpha} + \frac{\Delta\rho}{\rho}\right] + \left[\frac{1}{2}\frac{\Delta\alpha}{\alpha} - 4\left[\frac{\beta}{\alpha}\right]^2\frac{\Delta\beta}{\beta} - \right.$$

$$\left. - 2\left[\frac{\beta}{\alpha}\right]^2\frac{\Delta\rho}{\rho}\right]\sin^2\theta + \frac{\alpha}{2\alpha}\left(\tan^2\theta\sin^2\tan^2\theta\sin^2\theta\right) \quad (2)$$

Where are:

α – average P-wave velocity (m/s),
β – average S-wave velocity (m/s),
ρ – average density (g/cm^3),
$\Delta\alpha$ – difference in P-wave velocity (m/s),
$\Delta\beta$ – difference in S-wave velocity (m/s),
$\Delta\rho$ – difference in density (g/cm^3).

$$R(\theta) = I_p + G\sin^2\theta + F\left(\tan^2\theta - \tan^2\theta - \sin^2\theta\right) \quad (3)$$

Where are:

I_p – intercept,
G – gradient,
F – (1*Δv_p/2* Δv_s).

$$R_P(\theta) = dR_{P0} + eR_{s0} + f\frac{\Delta\rho}{\rho} \quad (4)$$

Where are:

d – (1+tan$^2\theta$),
e – (-8*v_s^2*sin$^2\theta$/v_p^2),
f – (2*v_s^2*sin$^2\theta$/v_p^2-tan$^2\theta$/2),
V_p – average P-wave velocity (m/s),
V_s – average S-wave velocity (m/s).

Commonly, linear regression analysis is conducted on seismic amplitudes at different offsets to estimate the intercept (Ip) and gradient (G). It should be noted that several attributes can be derived from Ip and G, including their product, scaled S-wave reflectivity, fluid factor, gas indicator, scaled Poisson reflectivity, energy-weighted, etc. (**Farfour et al., 2016; Farfour and Foster, 2021; Farfour and Foster, 2022**; **Ridwan et al., 2020**). The AVO attributes have also been utilized by **Sukmono et al. (2017)** in the preliminary shallow geohazard identification in a deep-water exploration area, Gulf of Mexico, using AVO attributes such as intercept, gradient, and product.

Several studies have utilised well data in reservoir characterization, as demonstrated by **Sari et al. (2018)** in the seismic anisotropy estimation of the Talang Akar Formation using ultrasonic tomography in core plugs. **Ambarsari et al. (2021)** investigated the effects of lithology and facies types on the anisotropy parameters and upscaling factor of the sand reservoirs in the deep-water Sadewa field, Kutei Basin, East Kalimantan, using core and log data from well data. This research aims to identify the differences in AVO responses in well data concerning the presence of CO_2 and compare them with other hydrocarbon fluids in the LTAF interval. Additionally, the study aims to analyse the changes in AVO attributes (intercept and gradient) in response to variations in CO_2 saturation through AVO modelling using well data in the hope of solving the CO_2 insitu problem to the production and development of this field.

2. Methods

AVO modelling is conducted to understand the AVO response in well data concerning the presence of CO_2. This modelling utilizes various well data, including log data (Density, Porosity, Vp & Vs Sonic/DT), Drill Stem Test (DST) data, well marker data resulting from stratigraphic sequence interpretation, and well reports. Wells with reservoir intervals containing CO_2 levels tabulated using DST data are used for AVO modelling. Wells without CO_2 reservoir intervals are also used as a comparison in this study.

AVO modelling is carried out by constructing a reflection coefficient versus angle curve using well log data (Density, Porosity, Vp & Vs Sonic/DT). The reflection coefficient is generated using AVO equations from **Aki and Richards (2002)**, **Wiggins et al. (1983)**, **Shuey (1985)**, and **Fatti et al. (1994)**. The reflection coefficient versus angle curve is utilized to analyse AVO responses and classify them according to the classification proposed by Rutherford and Williams (1989). The angle range employed in this study to accommodate the generated reflection coefficients is 0-45 degrees. The intercept and gradient from these AVO equations are also used to produce a crossplot of intercept vs. gradient with the aim of classifying Castagna's AVO responses (**Castagna et al., 1998**). This gradient analysis is conducted to obtain AVO responses for the LTAF formation in general, AVO responses to the presence of fluids (brine and hydrocarbons), and AVO responses to the presence of CO_2. Various AVO responses to these fluids will be compared with the presence of CO_2 to identify significant differences in CO_2 AVO responses.

Crossplot of AVO attributes is conducted to determine the sensitivity of AVO attributes to the presence of fluids, specifically in this research, CO_2. This research will utilize the crossplot method of AVO attributes using AVO modelling data from well data. The AVO attributes used are Intercept and Gradient. The data used to create

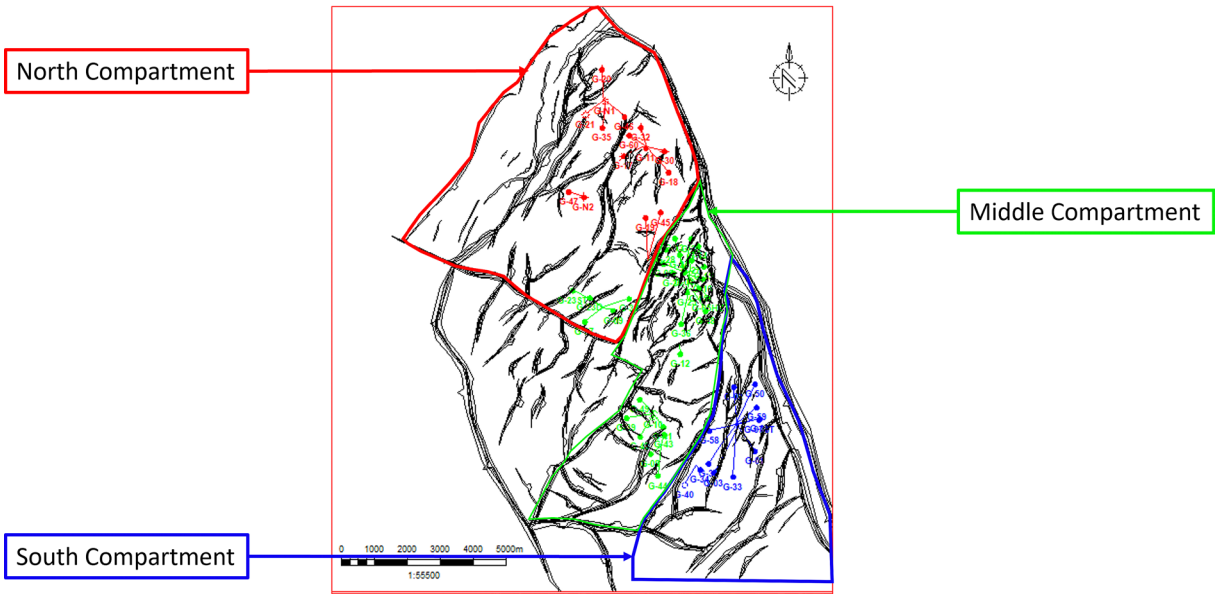

Figure 3: Compartmentalisation of the study area with three main compartements

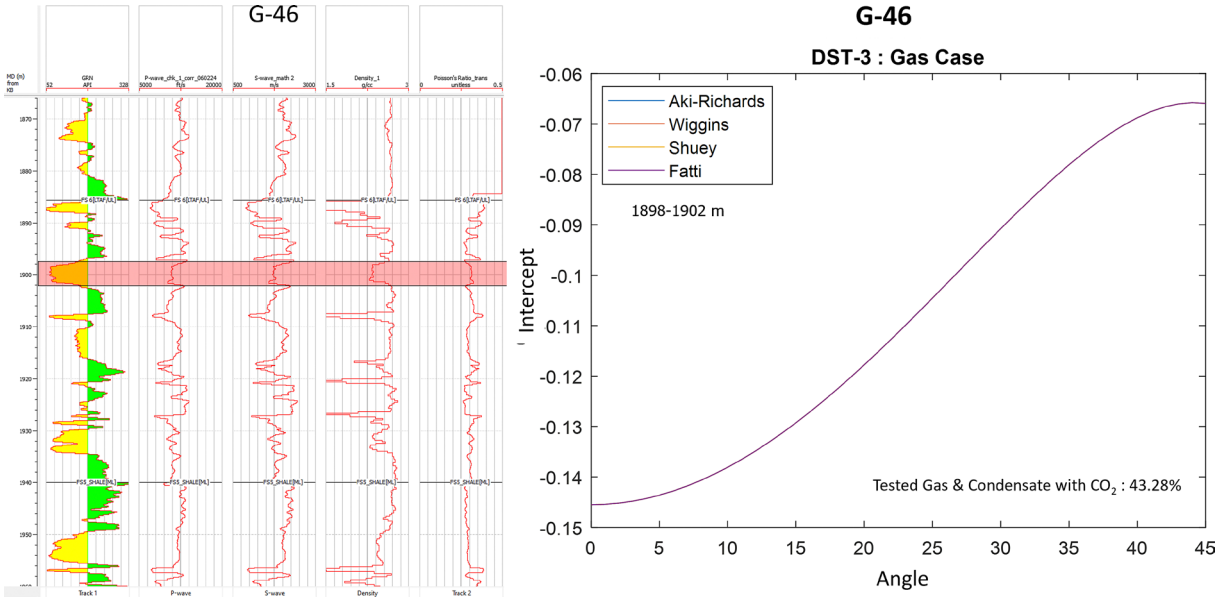

Figure 4: Log response of the target interval (left) and the results of synthetic gradient modelling in well G-46 DST-3 with intercept curves for each method (right)

the crossplot of AVO attributes are divided based on the interval of each stratigraphic sequence. Crossplotting AVO attributes is carried out within the same stratigraphic interval, assuming that a single sequence has a consistent facies distribution. The crossplot analysis is performed by examining the changes in AVO attribute responses, in this case, intercept and gradient, with variations in CO_2 saturation.

3. Results

The following are the results of the methodology explained in the previous chapter.

3.1 Synthetic Gradient Analysis

Synthetic gradient modelling analysis was conducted on several intervals of Drill Stem Test (DST) from each well. This modelling utilized corrected checkshot P-Wave log data, S-wave log data, and density log data. The modelling was performed using four AVO approximation equations from **Aki and Richard (2002)**, **Fatti et al. (1980)**, **Wiggins et al. (1983)**, and **Shuey (1985)**. The calculations from the four AVO equations above are performed using Matlab software, along with Microsoft Excel for quality control with manual calculations. Through these four equations, the obtained results had

Table 1: Results of synthetic gradient modelling in well G-46 DST-3 with intercept values for each angle in each method

Angle	MATLAB				EXCEL			
	Aki-Richard	Shuey	Fatti	Wiggins	Aki-Richard	Shuey	Fatti	Wiggins
0	-0.1455	-0.1455	-0.1455	-0.1455	-0.1455	-0.1455	-0.1455	-0.1455
1	-0.1454	-0.1454	-0.1454	-0.1454	-0.1455	-0.1455	-0.1455	-0.1455
2	-0.1452	-0.1452	-0.1452	-0.1452	-0.1452	-0.1452	-0.1452	-0.1452
3	-0.1448	-0.1448	-0.1448	-0.1448	-0.1448	-0.1448	-0.1448	-0.1448
4	-0.1443	-0.1443	-0.1443	-0.1443	-0.1443	-0.1443	-0.1443	-0.1443
5	-0.1436	-0.1436	-0.1436	-0.1436	-0.1436	-0.1436	-0.1436	-0.1436
6	-0.1428	-0.1428	-0.1428	-0.1428	-0.1428	-0.1428	-0.1428	-0.1428
7	-0.1418	-0.1418	-0.1418	-0.1418	-0.1418	-0.1418	-0.1418	-0.1418
8	-0.1407	-0.1407	-0.1407	-0.1407	-0.1407	-0.1407	-0.1407	-0.1407
9	-0.1395	-0.1395	-0.1395	-0.1395	-0.1395	-0.1395	-0.1395	-0.1395
10	-0.1381	-0.1381	-0.1381	-0.1381	-0.1381	-0.1381	-0.1381	-0.1381
11	-0.1366	-0.1366	-0.1366	-0.1366	-0.1366	-0.1366	-0.1366	-0.1366
12	-0.1349	-0.1349	-0.1349	-0.1349	-0.1349	-0.1349	-0.1349	-0.1349
13	-0.1331	-0.1331	-0.1331	-0.1331	-0.1332	-0.1332	-0.1332	-0.1332
14	-0.1313	-0.1313	-0.1313	-0.1313	-0.1313	-0.1313	-0.1313	-0.1313
15	-0.1293	-0.1293	-0.1293	-0.1293	-0.1293	-0.1293	-0.1293	-0.1293
16	-0.1271	-0.1271	-0.1271	-0.1271	-0.1272	-0.1272	-0.1272	-0.1272
17	-0.1249	-0.1249	-0.1249	-0.1249	-0.1250	-0.1250	-0.1250	-0.1250
18	-0.1226	-0.1226	-0.1226	-0.1226	-0.1227	-0.1227	-0.1227	-0.1227
19	-0.1202	-0.1202	-0.1202	-0.1202	-0.1203	-0.1203	-0.1203	-0.1203
20	-0.1178	-0.1178	-0.1178	-0.1178	-0.1178	-0.1178	-0.1178	-0.1178
21	-0.1152	-0.1152	-0.1152	-0.1152	-0.1152	-0.1152	-0.1152	-0.1152
22	-0.1126	-0.1126	-0.1126	-0.1126	-0.1126	-0.1126	-0.1126	-0.1126
23	-0.11	-0.11	-0.11	-0.11	-0.1100	-0.1100	-0.1100	-0.1100
24	-0.1073	-0.1073	-0.1073	-0.1073	-0.1073	-0.1073	-0.1073	-0.1073
25	-0.1045	-0.1045	-0.1045	-0.1045	-0.1045	-0.1045	-0.1045	-0.1045
26	-0.1018	-0.1018	-0.1018	-0.1018	-0.1018	-0.1018	-0.1018	-0.1018
27	-0.099	-0.099	-0.099	-0.099	-0.0990	-0.0990	-0.0990	-0.0990
28	-0.0962	-0.0962	-0.0962	-0.0962	-0.0962	-0.0962	-0.0962	-0.0962
29	-0.0935	-0.0935	-0.0935	-0.0935	-0.0935	-0.0935	-0.0935	-0.0935
30	-0.0907	-0.0907	-0.0907	-0.0907	-0.0908	-0.0908	-0.0908	-0.0908
31	-0.088	-0.088	-0.088	-0.088	-0.0881	-0.0881	-0.0881	-0.0881
32	-0.0854	-0.0854	-0.0854	-0.0854	-0.0855	-0.0855	-0.0855	-0.0855
33	-0.0829	-0.0829	-0.0829	-0.0829	-0.0829	-0.0829	-0.0829	-0.0829
34	-0.0804	-0.0804	-0.0804	-0.0804	-0.0804	-0.0804	-0.0804	-0.0804
35	-0.0781	-0.0781	-0.0781	-0.0781	-0.0781	-0.0781	-0.0781	-0.0781
36	-0.0759	-0.0759	-0.0759	-0.0759	-0.0759	-0.0759	-0.0759	-0.0759
37	-0.0738	-0.0738	-0.0738	-0.0738	-0.0738	-0.0738	-0.0738	-0.0738
38	-0.0719	-0.0719	-0.0719	-0.0719	-0.0719	-0.0719	-0.0719	-0.0719
39	-0.0702	-0.0702	-0.0702	-0.0702	-0.0702	-0.0702	-0.0702	-0.0702
40	-0.0687	-0.0687	-0.0687	-0.0687	-0.0688	-0.0688	-0.0688	-0.0688
41	-0.0675	-0.0675	-0.0675	-0.0675	-0.0676	-0.0676	-0.0676	-0.0676
42	-0.0666	-0.0666	-0.0666	-0.0666	-0.0666	-0.0666	-0.0666	-0.0666
43	-0.066	-0.066	-0.066	-0.066	-0.0660	-0.0660	-0.0660	-0.0660
44	-0.0658	-0.0658	-0.0658	-0.0658	-0.0658	-0.0658	-0.0658	-0.0658
45	-0.0659	-0.0659	-0.0659	-0.0659	-0.0659	-0.0659	-0.0659	-0.0659

Table 2: The difference in intercept values between calculations conducted using Matlab and Excel applications for each AVO equation

Angle	Aki-Richard			Shuey			Fatti			Wiggins		
	Excel	Matlab	Diff.	Excel	Matlab	Diff.	Excel	Matlab	Diff.	Excel	Matlab	Diff.
0	-0.146	-0.146	**2.62E-05**	-0.146	-0.146	**2.62E-05**	-0.146	-0.146	**2.62E-05**	-0.146	-0.146	**2.62E-05**
1	-0.145	-0.145	**5.04E-05**	-0.145	-0.145	**5.04E-05**	-0.145	-0.145	**5.04E-05**	-0.145	-0.145	**5.04E-05**
2	-0.145	-0.145	**2.31E-05**	-0.145	-0.145	**2.31E-05**	-0.145	-0.145	**2.31E-05**	-0.145	-0.145	**2.31E-05**
3	-0.145	-0.145	**4.49E-05**	-0.145	-0.145	**4.49E-05**	-0.145	-0.145	**4.49E-05**	-0.145	-0.145	**4.49E-05**
4	-0.144	-0.144	**1.68E-05**	-0.144	-0.144	**1.68E-05**	-0.144	-0.144	**1.68E-05**	-0.144	-0.144	**1.68E-05**
5	-0.144	-0.144	**4.01E-05**	-0.144	-0.144	**4.01E-05**	-0.144	-0.144	**4.01E-05**	-0.144	-0.144	**4.01E-05**
6	-0.143	-0.143	**1.66E-05**	-0.143	-0.143	**1.66E-05**	-0.143	-0.143	**1.66E-05**	-0.143	-0.143	**1.66E-05**
7	-0.142	-0.142	**4.84E-05**	-0.142	-0.142	**4.84E-05**	-0.142	-0.142	**4.84E-05**	-0.142	-0.142	**4.84E-05**
8	-0.141	-0.141	**3.80E-05**	-0.141	-0.141	**3.80E-05**	-0.141	-0.141	**3.80E-05**	-0.141	-0.141	**3.80E-05**
9	-0.139	-0.140	**-1.16E-05**	-0.139	-0.140	**-1.16E-05**	-0.139	-0.140	**-1.16E-05**	-0.139	-0.140	**-1.16E-05**
10	-0.138	-0.138	**2.72E-06**	-0.138	-0.138	**2.72E-06**	-0.138	-0.138	**2.72E-06**	-0.138	-0.138	**2.72E-06**
11	-0.137	-0.137	**-1.52E-05**	-0.137	-0.137	**-1.52E-05**	-0.137	-0.137	**-1.52E-05**	-0.137	-0.137	**-1.52E-05**
12	-0.135	-0.135	**3.88E-05**	-0.135	-0.135	**3.88E-05**	-0.135	-0.135	**3.88E-05**	-0.135	-0.135	**3.88E-05**
13	-0.133	-0.133	**6.93E-05**	-0.133	-0.133	**6.93E-05**	-0.133	-0.133	**6.93E-05**	-0.133	-0.133	**6.93E-05**
14	-0.131	-0.131	**-1.90E-05**	-0.131	-0.131	**-1.90E-05**	-0.131	-0.131	**-1.90E-05**	-0.131	-0.131	**-1.90E-05**
15	-0.129	-0.129	**-2.04E-05**	-0.129	-0.129	**-2.04E-05**	-0.129	-0.129	**-2.04E-05**	-0.129	-0.129	**-2.04E-05**
16	-0.127	-0.127	**7.07E-05**	-0.127	-0.127	**7.07E-05**	-0.127	-0.127	**7.07E-05**	-0.127	-0.127	**7.07E-05**
17	-0.125	-0.125	**6.06E-05**	-0.125	-0.125	**6.06E-05**	-0.125	-0.125	**6.06E-05**	-0.125	-0.125	**6.06E-05**
18	-0.123	-0.123	**5.60E-05**	-0.123	-0.123	**5.60E-05**	-0.123	-0.123	**5.60E-05**	-0.123	-0.123	**5.60E-05**
19	-0.120	-0.120	**6.41E-05**	-0.120	-0.120	**6.41E-05**	-0.120	-0.120	**6.41E-05**	-0.120	-0.120	**6.41E-05**
20	-0.118	-0.118	**-7.40E-06**	-0.118	-0.118	**-7.40E-06**	-0.118	-0.118	**-7.40E-06**	-0.118	-0.118	**-7.40E-06**
21	-0.115	-0.115	**4.96E-05**	-0.115	-0.115	**4.96E-05**	-0.115	-0.115	**4.96E-05**	-0.115	-0.115	**4.96E-05**
22	-0.113	-0.113	**4.38E-05**	-0.113	-0.113	**4.38E-05**	-0.113	-0.113	**4.38E-05**	-0.113	-0.113	**4.38E-05**
23	-0.110	-0.110	**-1.57E-05**	-0.110	-0.110	**-1.57E-05**	-0.110	-0.110	**-1.57E-05**	-0.110	-0.110	**-1.57E-05**
24	-0.107	-0.107	**-1.90E-05**	-0.107	-0.107	**-1.90E-05**	-0.107	-0.107	**-1.90E-05**	-0.107	-0.107	**-1.90E-05**
25	-0.105	-0.105	**4.42E-05**	-0.105	-0.105	**4.42E-05**	-0.105	-0.105	**4.42E-05**	-0.105	-0.105	**4.42E-05**
26	-0.102	-0.102	**-1.52E-05**	-0.102	-0.102	**-1.52E-05**	-0.102	-0.102	**-1.52E-05**	-0.102	-0.102	**-1.52E-05**
27	-0.099	-0.099	**1.45E-05**	-0.099	-0.099	**1.45E-05**	-0.099	-0.099	**1.45E-05**	-0.099	-0.099	**1.45E-05**
28	-0.096	-0.096	**4.55E-05**	-0.096	-0.096	**4.55E-05**	-0.096	-0.096	**4.55E-05**	-0.096	-0.096	**4.55E-05**
29	-0.093	-0.094	**-9.18E-06**	-0.093	-0.094	**-9.18E-06**	-0.093	-0.094	**-9.18E-06**	-0.093	-0.094	**-9.18E-06**
30	-0.091	-0.091	**6.43E-05**	-0.091	-0.091	**6.43E-05**	-0.091	-0.091	**6.43E-05**	-0.091	-0.091	**6.43E-05**
31	-0.088	-0.088	**8.05E-05**	-0.088	-0.088	**8.05E-05**	-0.088	-0.088	**8.05E-05**	-0.088	-0.088	**8.05E-05**
32	-0.085	-0.085	**5.50E-05**	-0.085	-0.085	**5.50E-05**	-0.085	-0.085	**5.50E-05**	-0.085	-0.085	**5.50E-05**
33	-0.083	-0.083	**4.35E-06**	-0.083	-0.083	**4.35E-06**	-0.083	-0.083	**4.35E-06**	-0.083	-0.083	**4.35E-06**
34	-0.080	-0.080	**4.60E-05**	-0.080	-0.080	**4.60E-05**	-0.080	-0.080	**4.60E-05**	-0.080	-0.080	**4.60E-05**
35	-0.078	-0.078	**-1.33E-06**	-0.078	-0.078	**-1.33E-06**	-0.078	-0.078	**-1.33E-06**	-0.078	-0.078	**-1.33E-06**
36	-0.076	-0.076	**-1.77E-05**	-0.076	-0.076	**-1.77E-05**	-0.076	-0.076	**-1.77E-05**	-0.076	-0.076	**-1.77E-05**
37	-0.074	-0.074	**1.83E-05**	-0.074	-0.074	**1.83E-05**	-0.074	-0.074	**1.83E-05**	-0.074	-0.074	**1.83E-05**
38	-0.072	-0.072	**2.93E-05**	-0.072	-0.072	**2.93E-05**	-0.072	-0.072	**2.93E-05**	-0.072	-0.072	**2.93E-05**
39	-0.070	-0.070	**4.01E-05**	-0.070	-0.070	**4.01E-05**	-0.070	-0.070	**4.01E-05**	-0.070	-0.070	**4.01E-05**
40	-0.069	-0.069	**7.69E-05**	-0.069	-0.069	**7.69E-05**	-0.069	-0.069	**7.69E-05**	-0.069	-0.069	**7.69E-05**
41	-0.068	-0.068	**6.82E-05**	-0.068	-0.068	**6.82E-05**	-0.068	-0.068	**6.82E-05**	-0.068	-0.068	**6.82E-05**
42	-0.067	-0.067	**4.48E-05**	-0.067	-0.067	**4.48E-05**	-0.067	-0.067	**4.48E-05**	-0.067	-0.067	**4.48E-05**
43	-0.066	-0.066	**4.00E-05**	-0.066	-0.066	**4.00E-05**	-0.066	-0.066	**4.00E-05**	-0.066	-0.066	**4.00E-05**
44	-0.066	-0.066	**-9.78E-06**	-0.066	-0.066	**-9.78E-06**	-0.066	-0.066	**-9.78E-06**	-0.066	-0.066	**-9.78E-06**
45	-0.066	-0.066	**3.51E-05**	-0.066	-0.066	**3.51E-05**	-0.066	-0.066	**3.51E-05**	-0.066	-0.066	**3.51E-05**

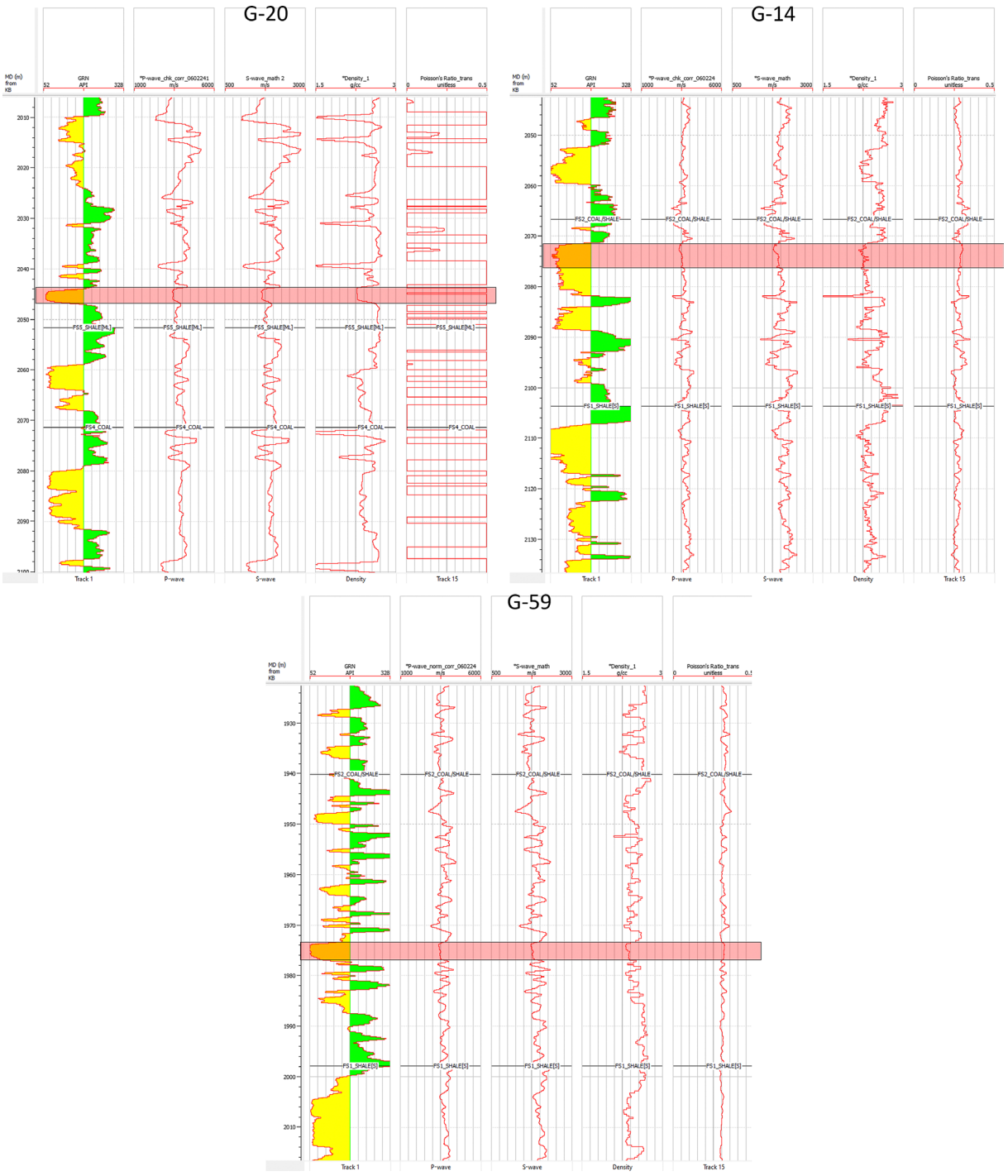

Figure 5: One example of the log response of the target interval for synthetic AVO gradient modelling on well data in the northern (north), central (middle), and southern (south) compartments

the same reflectivity values, in other words, they had the same intercept values at all angles (see **Figure 4** and **Table 1**). It should be noted that the QC calculation results using Excel are nearly identical to those using Matlab (difference < 8.05E-05, indicating the accuracy of the Matlab calculations (see **Table 2**). This AVO response is generated by the log response as depicted in **Figure 4**. In the target interval, the log responses of p-wave, s-wave, and density are smaller compared to the shale layers above them. These responses are associated with low Gamma-Ray values, indicating a sand lithology.

Through this synthetic AVO gradient modelling, the overall response of the LTAF interval in the research area can be determined (see **Table 3**). From the four equations explained in the previous chapter, the AVO responses obtained are the same. Therefore, the equation used subsequently to obtain the intercept and gradient values is **Equation 3**. The AVO responses obtained are

Table 3: Results of synthetic AVO gradient modelling in the LTAF interval

Compartement	Well	Test No.	Formation (LTAF)	Mol % CO2	Fluid Type	AVO Modelling CLASS
North 1	G-20	DST#4	FS6	22.4	Gas	4
North 1	G-20	DST#3	FS6	43.38	Gas	4
North 1	G-21	DST#2	FS5	20	Gas	4
North 1	G-21	DST#1	FS4	34.09	Gas	1
North 1	G-35	DST#1	FS4	18	Gas	4
North 1	G-46	DST#2	FS4	19	Gas	4
North 1	G-46	DST#3	FS6	7	Gas	4
North 1	G-N1	DST#6	FS5	19.09	Gas	4
North 1	G-N1	DST#5	FS4	39.97	Gas	4
North 2	G-11	DST#2	FS5	15	Oil & Gas	3
North 2	G-11	DST#1	FS4	30	Gas	4
North 2	G-17	DST#1	FS2	41.45	Gas	4
North 2	G-17	DST#3	FS3	19.04	Water, Oil, Gas, CO2	4
North 2	G-17	DST#5	FS4	12.67	Gas	2
North 2	G-17	DST#2	FS2	29.62	Gas	4
North 2	G-17	DST#4	FS4	17.14	Gas	4
North 2	G-18	DST#2	FS4	11.26	Gas	4
North 2	G-30	DST#2	FS5	-	Oil	1
North 2	G-60	DST#3	FS3	-	Water & Oil	1
North 2	G-60	DST#4	FS5	8	Gas	4
North 4	G-19	DST#6	FS6	11.31	Gas	4
North 4	G-45	DST#3	FS6	7	Gas	4
Middle 1	G-14	DST#2	FS2	50	Gas	4
Middle 1	G-24	DST#2	FS2	-	Gas	4
Middle 1	G-24	DST#3	FS4	-	Gas	1
Middle 1	G-29	DST#2	FS2	-	Gas	4
Middle 1	G-4	DST#4	FS4	11.84	Gas	4
Middle 1 Fault	G-28	DST#3	FS2	40	Gas	4
Middle 1 Fault	G-28	DST#2	FS2	45	Gas	4
Middle 2	G-27	DST#5	FS3	50	Gas	4
Middle 2	G-36	DST#3	FS3	37	Gas	4
Middle 3	G-23 ST	DST#3	FS5	8.14	Gas	4
Middle 3	G-37	DST#1	FS5	6	Gas	4
Middle 3	G-38	DST#2	FS3	36	Gas	4
Middle 3	G-38	DST#3	FS3	36	Gas	4
Middle 3	G-9	DST#2	FS3	25	Gas	3
Middle 4	G-10	DST#1	FS5	4	Gas	4
Middle 4	G-10	DST#2	FS5	8	Gas	3
Middle 4	G-39	DST#2	FS3	16	Gas	4
Middle 4	G-41	DST#3	FS5	7	Gas	4
Middle 4	G-41	DST#2	FS5	7	Gas	4
Middle 4	G-42	DST#2	FS3	14	Oil & Gas	4
Middle 4	G-49	DST#2	FS6	18	Gas	1
Middle 4	G-49	DST#3	FS6	12	Gas	1
Middle 5	G-43	DST#4	FS5	4	Gas	4
Middle 5	G-44	DST#3	FS5	5	Gas	4
South 1	G-1	DST#5	FS6	6.97	Oil & Gas	4

Table 3: Continued

Compartement	Well	Test No.	Formation (LTAF)	Mol % CO2	Fluid Type	AVO Modelling CLASS
South 1	G-1	DST#3	FS4	15.05	Water, Oil, Gas, CO2	4
South 1	G-1	DST#2	FS2	33.45	Oil & Gas	4
South 1	G-2	DST#3	FS4	22.02	Oil & Gas	4
South 1	G-2	DST#4	FS5	8.13	Oil & Gas	2
South 1	G-2	DST#2	FS2	41.5	Gas	4
South 1	G-3	DST#1	FS4	7.47	**Oil**	3
South 1	G-3	DST#2	FS4	10.16	Water, Oil, & Gas	3
South 1	G-3	DST#3A	FS6	8.34	Gas	3
South 1	G-31	DST#4	FS4	-	Water	4
South 1	G-31	DST#1	FS2	-	Water	4
South 1	G-31	DST#6	FS5	9	Gas	4
South 1	G-33	DST#2	FS4	6	Gas	2
South 1	G-33	DST#1	FS2	-	Water & Oil	4
South 1	G-58	DST#1	FS2	20	Oil	4
South 1	G-58	DST#2	FS3	18	Oil & Gas	4
South 1	G-58	DST#3	FS3	20	Oil & Gas	4
South 1	G-59	DST#1	FS2	23	Gas	4
South 1	G-59	DST#3	FS3	15	Gas	4
South 1	G-59	DST#2	FS2	15	Gas	4

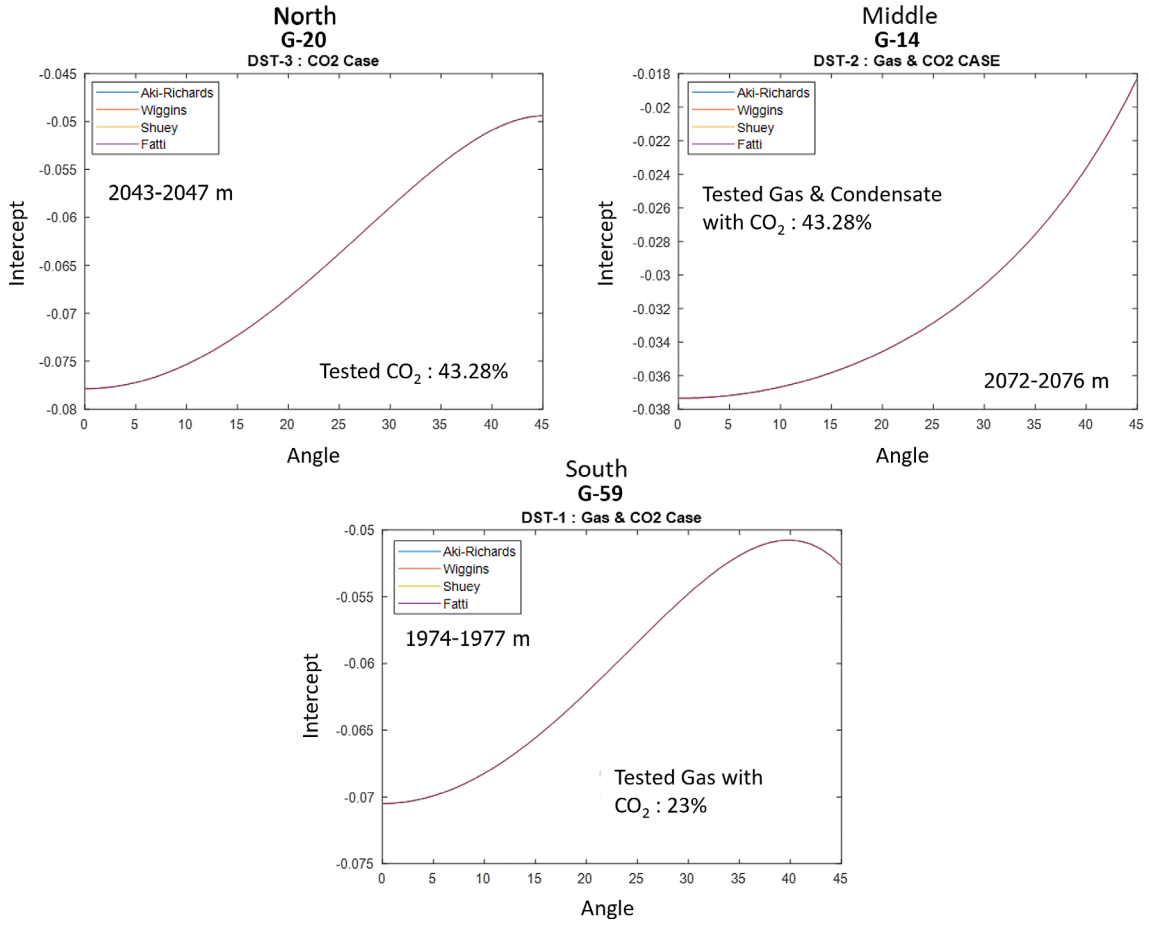

Figure 6: One example of the results of synthetic AVO gradient modelling on well data in the northern (north), central (middle), and southern (south) compartments

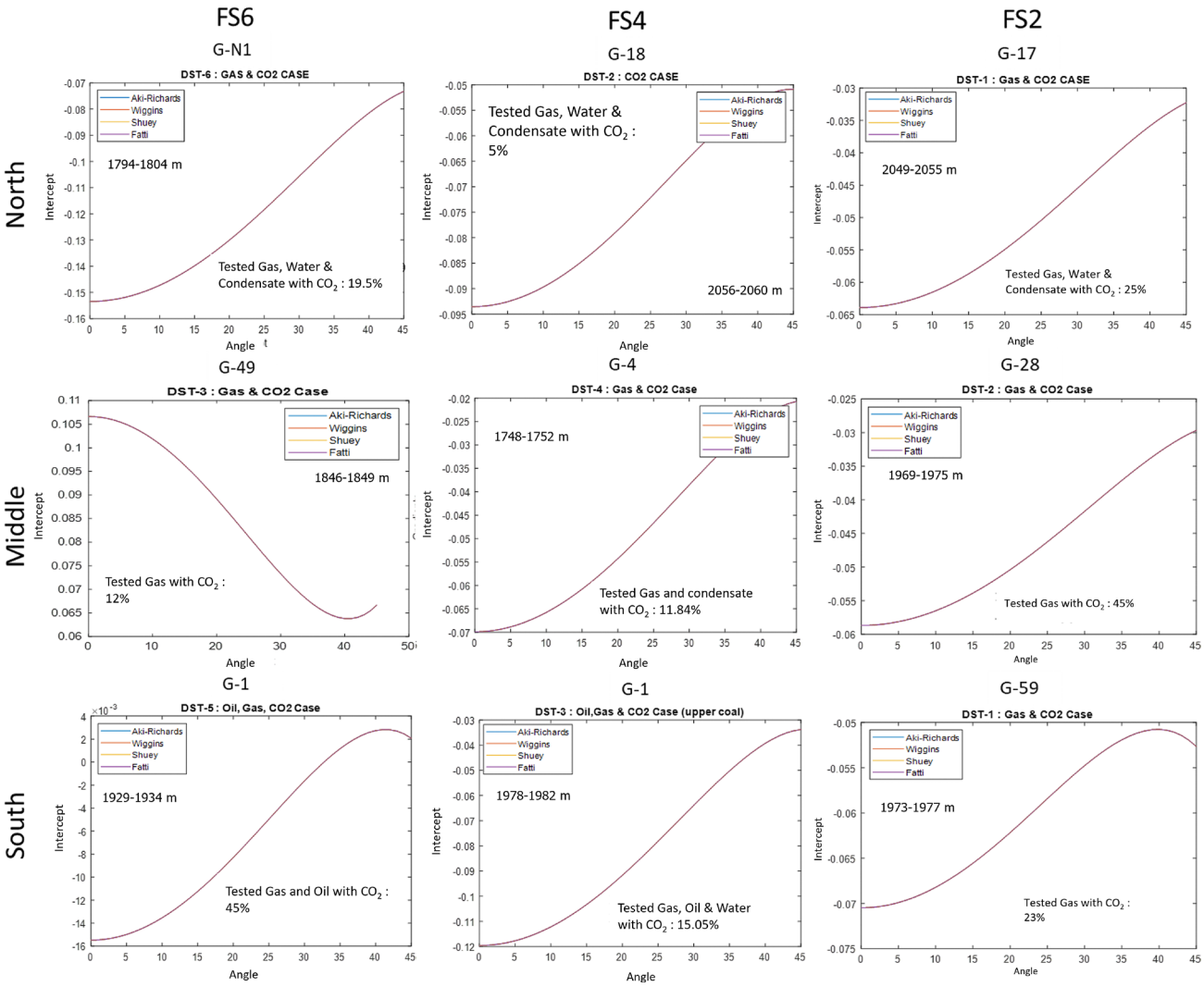

Figure 7: Results of synthetic AVO gradient modelling in the flooding surface intervals according to their compartmental areas

divided into three main compartments (see **Figure 3**). The analysis involves comparing the flooding surface intervals and the same compartments. In the northern compartment of this research area, the dominant AVO class obtained from 22 DST samples is class 4 AVO. Meanwhile, for the central compartment, the dominant AVO class obtained from 24 DST samples is class 4 AVO, and for the southern compartment, the dominant AVO class obtained from 20 DST samples is class 4 AVO (see **Figure 6**). The log responses of each sample from those three compartments are depicted in **Figure 5**. In the target interval for all of those samples, the log responses of p-wave, s-wave, and density are smaller compared to the shale layers above them. These responses are associated with low Gamma-Ray values, indicating a sand lithology.

If a comparison is made based on the difference in flooding surface, in the northern part, the shallowest interval FS6 has class 4 AVO, and subsequently, progressing to the deepest, FS4 has class 4 AVO with two samples of class 1 and 2, and FS2 has class 4 AVO. For the central compartment, in the FS6 interval, there is class 1 AVO, FS4 has class 4 AVO, and FS2 has class 4 AVO. Meanwhile, for the southern compartment, in the FS6 interval, there are class 4 and class 3 AVO, FS4 has class 4 AVO with three samples of class 2 and 3 AVO, and FS2 has class 4 AVO. Therefore, it can be said that in the LTAF formation, the dominant AVO class is class 4 AVO (see **Figure 7**).

3.2 Comparison of CO_2 with Hydrocarbon Fluids

This process is carried out with the aim of finding correlations between AVO attributes and CO_2 content and comparing it with other fluids, as well as the percentage of CO_2 presence. Firstly, a comparison analysis is conducted between CO_2 and other fluids using AVO attributes. This analysis is performed using well data located in the same compartment, the same sub-compartment, and the same flooding surface.

In the northern compartment, northern sub-compartment 2, flooding surface 3 (FS3), wells G-17 and G-60

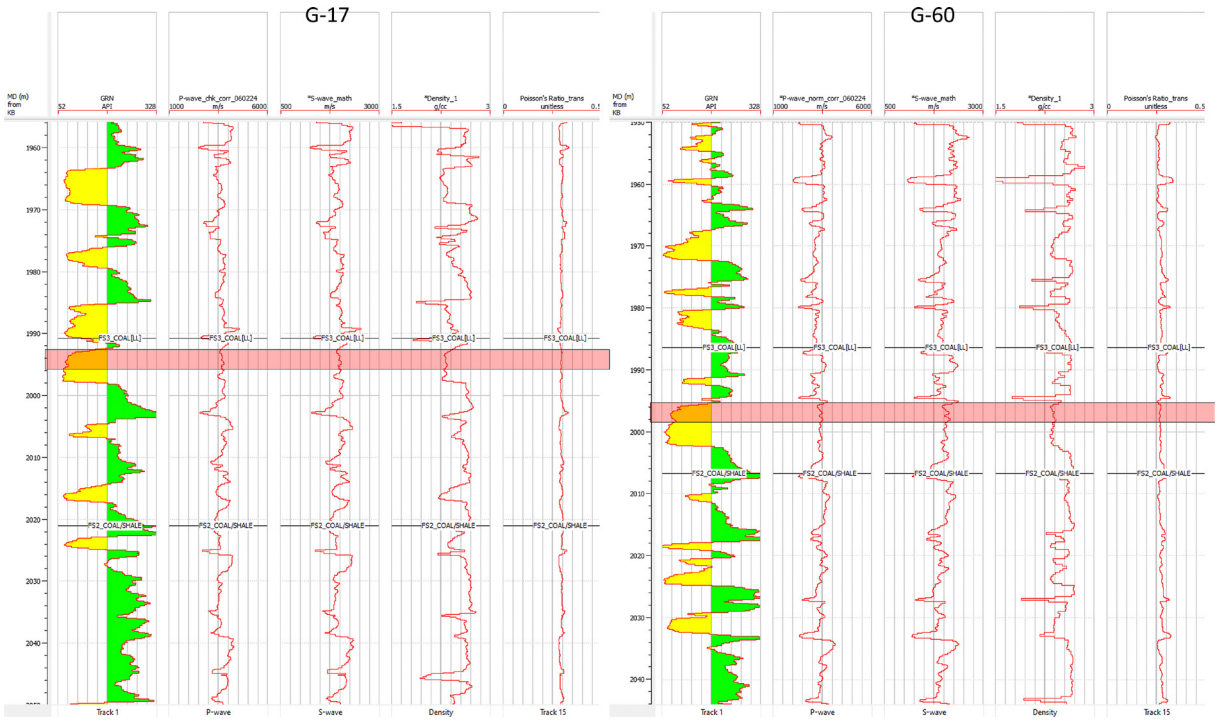

Figure 8: Log response of the target interval for synthetic AVO gradient modelling on well G-17 and G-60

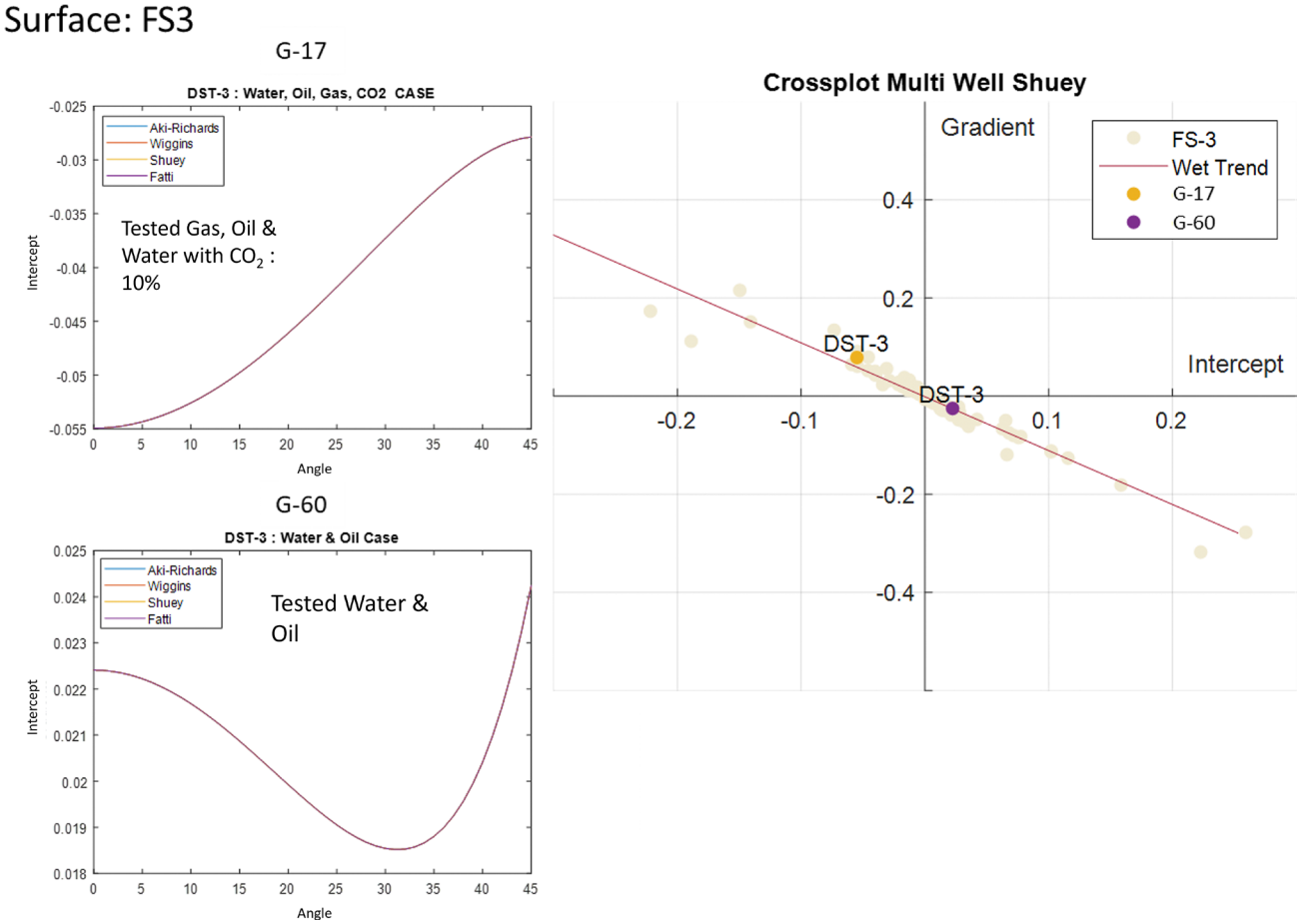

Figure 9: Crossplot intercept and gradient for wells G-17 and G-60

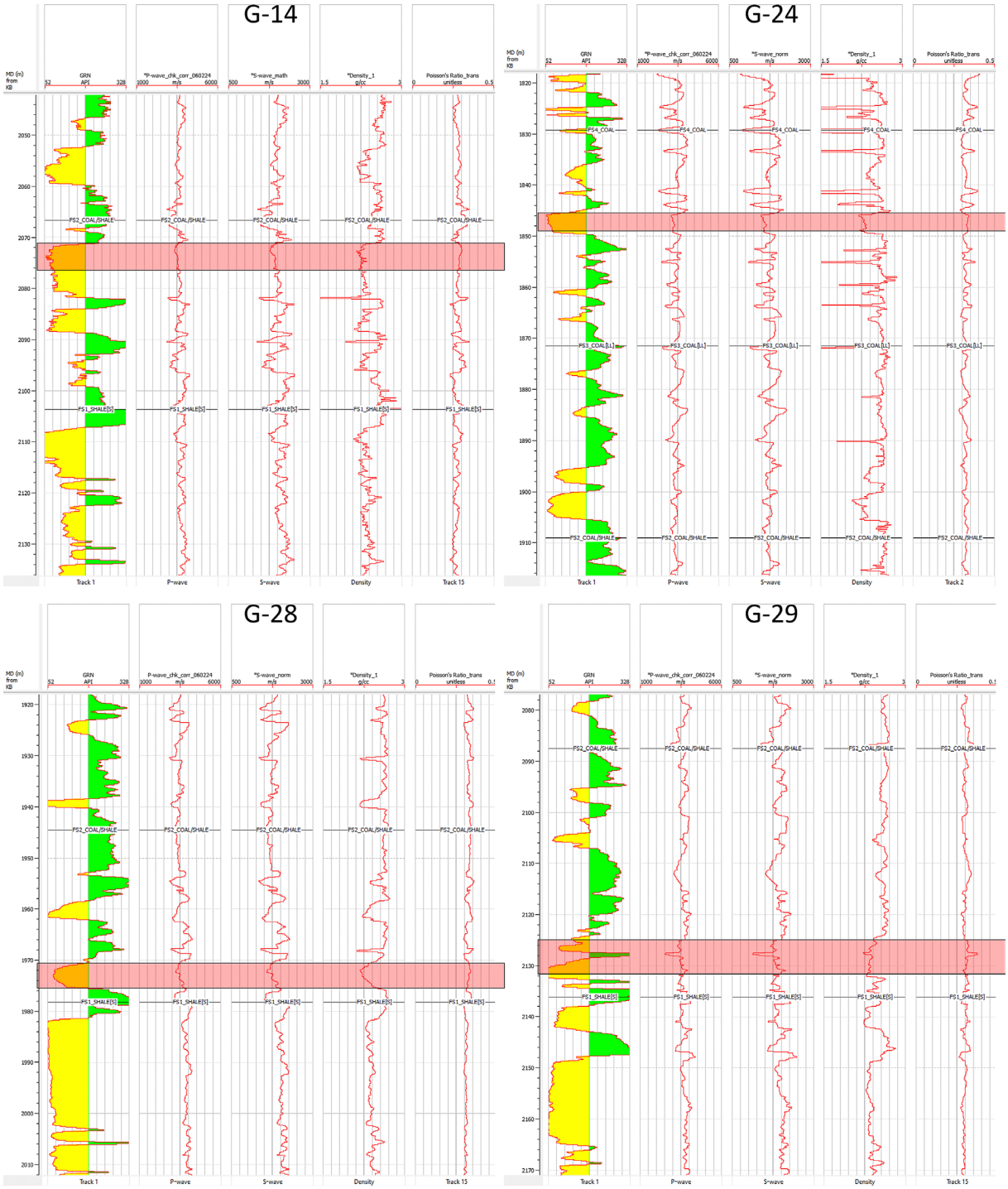

Figure 10: log response of the target interval for synthetic AVO gradient modelling on well G-14, G-24, G-28, and G-29

are used for AVO response comparison analysis (see **Figure 9**). Well G-17, through DST data, has a 10% CO_2 fluid content, while well G-60, through DST data, has water as the fluid content. The intercept and gradient attributes are crossplotted, showing that the AVO response from well G-17 is classified as class 4 AVO, whereas well G-60 has a class 2 AVO classification. The log response also exhibits a distinct pattern for each of the samples (see **Figure 8**). While the interval of sample G-17 displays p-wave, s-wave, and density logs smaller compared to the shale layers above them, the interval of sample G-60 shows the opposite trend, with p-wave and s-wave logs being larger and density being smaller than the shale layers above them.

In the central compartment, central sub-compartment 1, flooding surface 2 (FS2), wells G-14, G-24, G-28, and G-29 are used for AVO response comparison analysis. Well G-14, through DST data, has a 50% CO_2 fluid content, well G-24 has dry gas as the fluid content, well G-28 has a 45% CO_2 fluid content, and well G-29 has

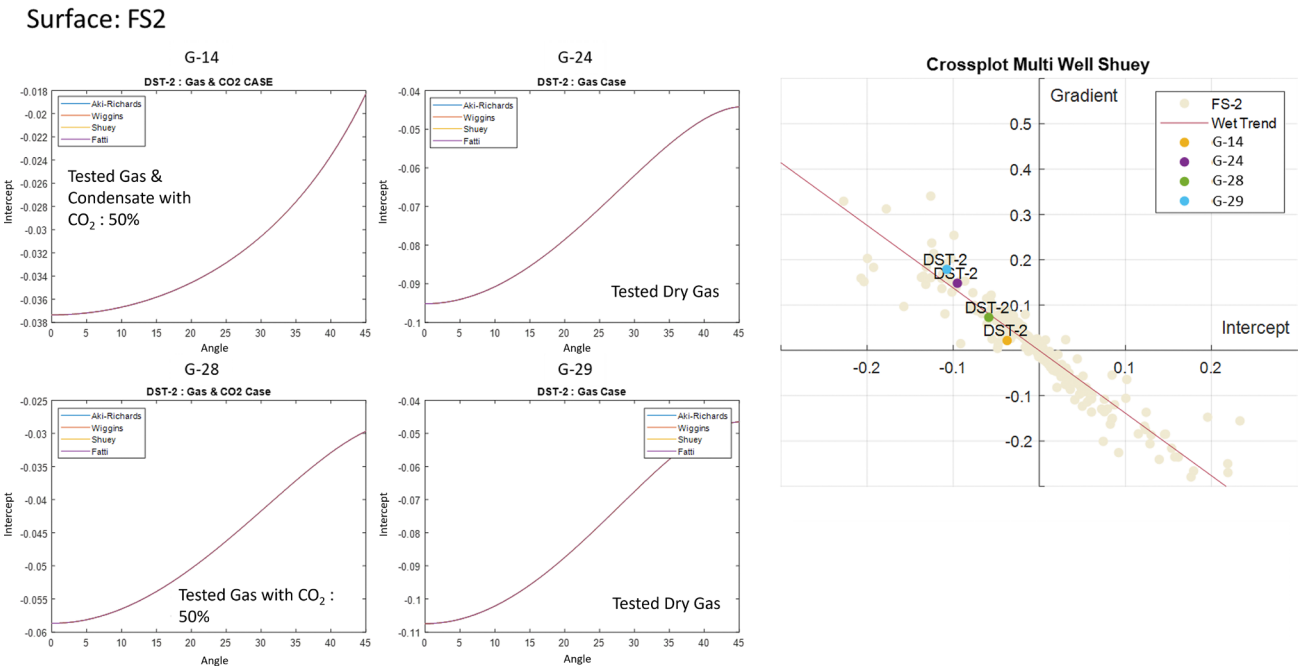

Figure 11: Crossplot intercept and gradient for wells G-14, G-24, G-28 and G-60

dry gas as the fluid content. The intercept and gradient attributes are crossplotted, indicating that the AVO response from the entire well data shows a class 4 AVO response. However, samples with CO_2 content have a more positive intercept and a more negative gradient, approaching the wet trend (see **Figure 11**). If we examine the **Figure 10**, it can be observed that in the interval of CO_2 DST samples (G-14 & G-28), the log responses of p-wave, s-wave, and density are smaller compared to the shale layers above them, as well as in the case of dry gas samples (G-24 & G-29). However, the CO_2 samples exhibit differences in the values of p-wave, s-wave, and density logs with the shale layer above, which are smaller compared to the dry gas samples.

In the southern compartment, southern sub-compartment 1, flooding surface 4 (FS4), wells G-3, G-31, and G-1 are used for AVO response comparison analysis (see **Figure 13**). Well G-3, through DST data, has a 10.16% CO_2 and 1.059 MMSCFD gas content, well G-31 has water as the fluid content, and well G-1 has a 15.05% CO_2 and 3320 MSCFD gas content. The intercept and gradient attributes are crossplotted, indicating that the AVO response from well G-1 and well G-31 shows a class 4 AVO response, while well G-3 has a class 3 AVO response. The log responses exhibit varying patterns among the three samples (see **Figure 12**). In the DST sample intervals of G-01 and G-31, the p-wave, s-wave, and density logs show smaller responses compared to the shale layers above, whereas the G-31 sample interval demonstrates log responses that are nearly identical to the shale layer above. The G-03 sample interval shows smaller p-wave and density log responses and larger s-wave responses compared to the shale layer above, resulting in an AVO classification of class 3.

3.3 The Influence of Changes in CO_2 Percentage on AVO Attributes

The influence of AVO attributes on fluid content has a quite significant effect, as discussed in the previous subsection. Each fluid has different physical properties, ranging from density, P-wave velocity to its Poisson's ratio. These differences in physical properties can lead to varied AVO responses, even with the same fluid content, such as CO_2. This can be observed using crossplots of intercept and gradient attributes for each percentage of CO_2 presence (see **Figure 10**).

In the northern compartment, flooding surface 6 (FS6), a comparison of CO_2 percentages is conducted between wells G-46, G-19, and G-20 using a crossplot of intercept and gradient (see **Figure 14**). It can be observed that as the percentage of CO_2 increases, its intercept value becomes more positive, and the gradient value becomes more negative, or the change tends towards class 2 AVO. The trend of these changes is similar at flooding surface 4 (FS4). Wells used for comparing CO_2 percentages in the crossplot of intercept and gradient are wells G-18, G-46, and G-N1 (see **Figure 14**). It can be seen that as the percentage of CO_2 increases, its intercept value becomes more positive, and the gradient value becomes more negative, or the change tends towards class 2 AVO.

In the central compartment, flooding surface 5 (FS5), a comparison of CO_2 percentages is conducted between wells G-43, G-44, and G-23ST using a crossplot of intercept and gradient (see **Figure 15**). It can be observed that as the percentage of CO_2 increases, its intercept value becomes more positive, and the gradient value becomes more negative, or the change tends towards class

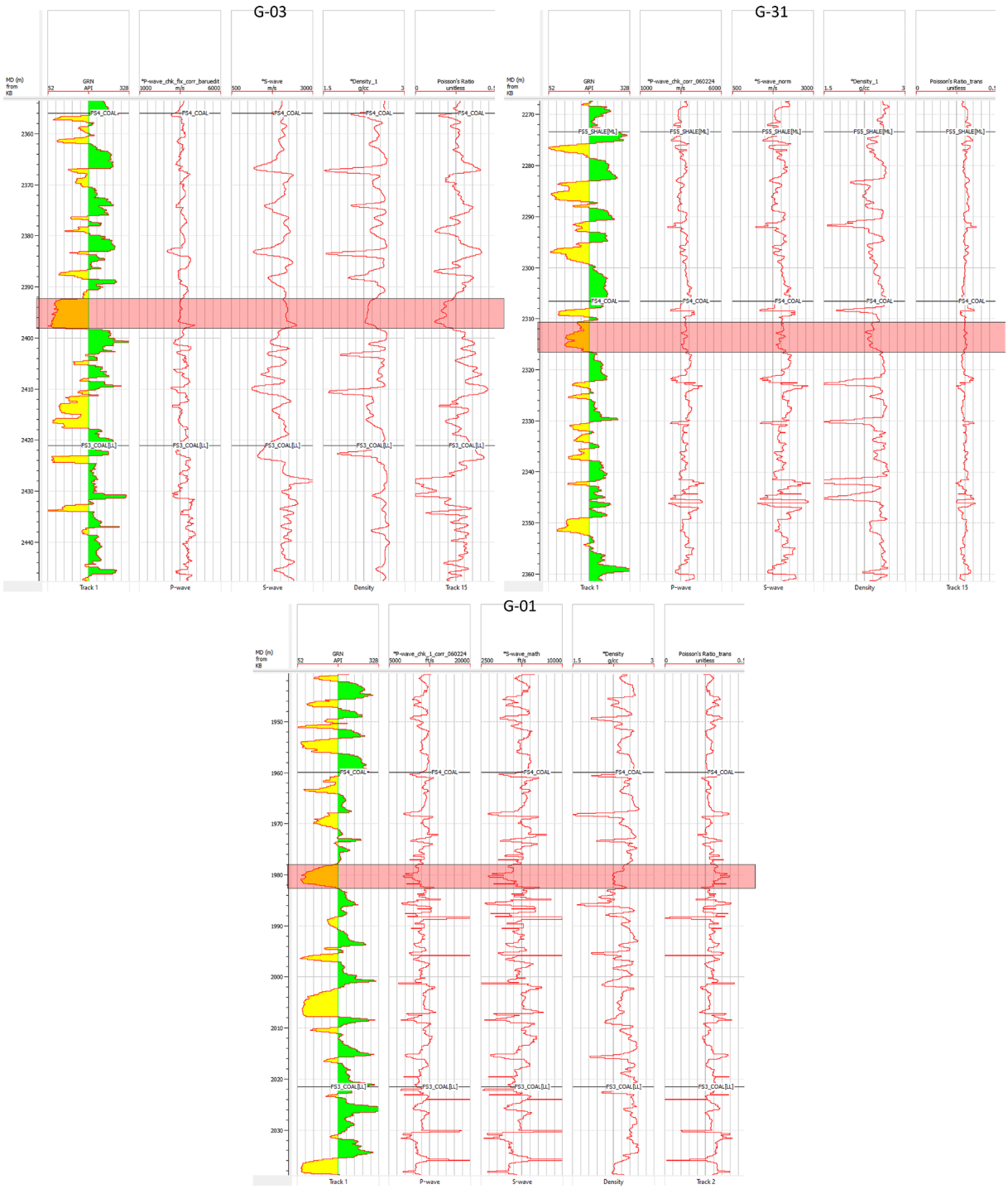

Figure 12: log response of the target interval for synthetic AVO gradient modelling on well G-03, G-31, and G-01

2 AVO. The trend of these changes is similar at flooding surface 3 (FS3). Wells used for comparing CO_2 percentages in the crossplot of intercept and gradient are wells G-42, G-36, and G-27 (see **Figure 15**). It can be seen that as the percentage of CO_2 increases, its intercept value becomes more positive, and the gradient value becomes more negative, or the change tends towards class 2 AVO.

In the southern compartment, flooding surface 4 (FS4), a comparison of CO_2 percentages is conducted between wells G-1 and G-2 using a crossplot of intercept and gradient (see **Figure 16**). It can be observed that as the percentage of CO_2 increases, its intercept value becomes more positive, and the gradient value becomes more negative, or the change tends towards class 2 AVO. The trend of these changes is similar at flooding surface 2 (FS2). Wells used for comparing CO_2 percentages in the crossplot of intercept and gradient are wells G-58, G-59, and G-2 (see **Figure 16**). It can be seen that as the percentage of CO_2 increases, its intercept value becomes

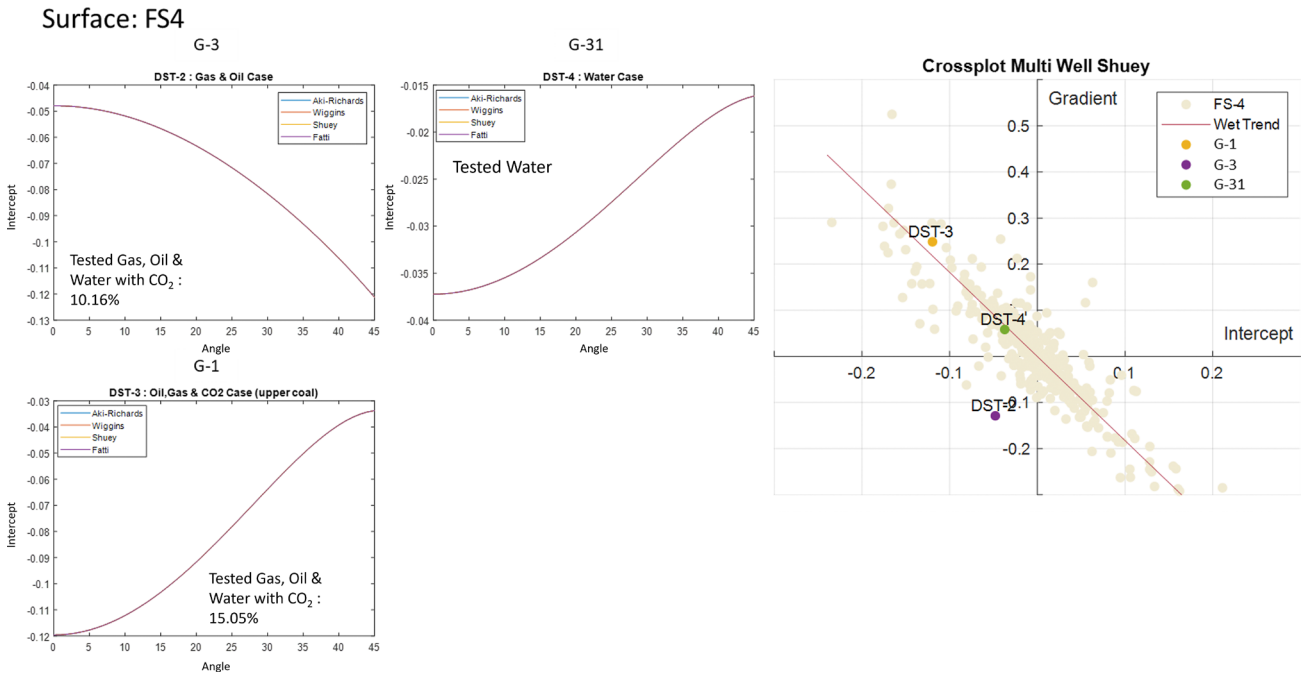

Figure 13: Crossplot intercept and gradient for wells G-3, G-31, and G-1

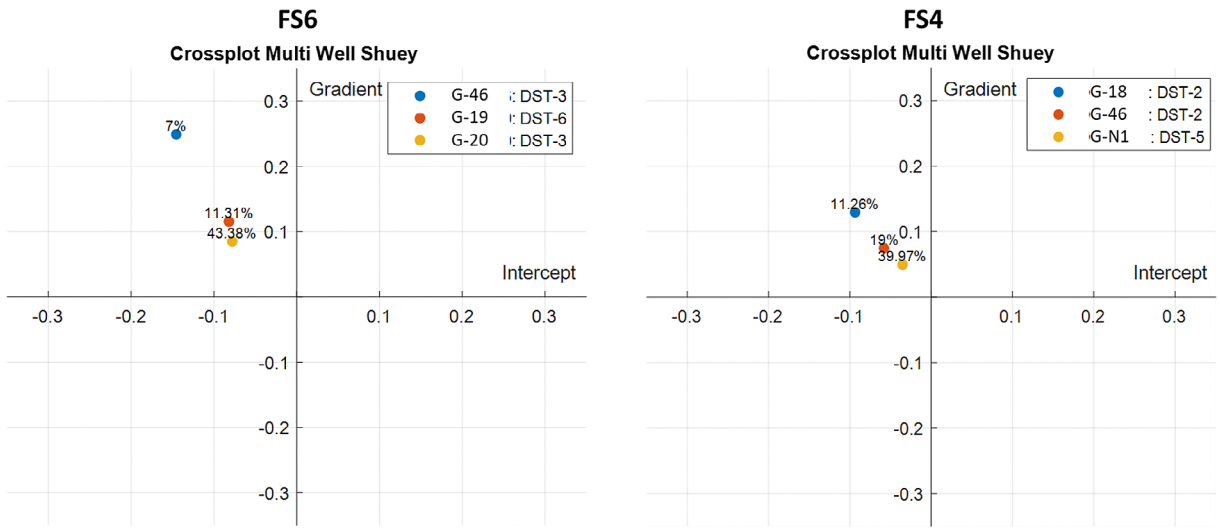

Well	DST	Intercept	Gradient	CO2 (%)
G-46	DST-3	-0.145499588	0.248991948	7
G-19	DST-6	-0.081857418	0.115424655	11.31
G-20	DST-3	-0.077871192	0.085049591	43.38

Well	DST	Intercept	Gradient	CO2 (%)
G-18	DST-2	-0.093548	0.1294659	11.26
G-46	DST-2	-0.058078	0.0746304	19
G-N1	DST-5	-0.035233	0.0497319	39.97

Figure 14: Crossplot of intercept and gradient attributes and their influence on changes in the percentage of CO_2 presence in the northern compartment

more positive, and the gradient value becomes more negative, or the change tends towards class 2 AVO. For all flooding surface intervals and compartments, it can be observed that AVO attributes such as intercept and gradient exhibit a consistent response, namely an increase in intercept and a decrease in gradient with the increasing CO_2 percentage (see **Table 4**).

4. Discussion

The results of this study, as explained in the preceding chapter, indicate that AVO responses can vary depending on the fluids present in the examined samples. As discussed in subsection 3.2, comparing CO_2 with other hydrocarbon fluids, in the northern compartment, north-

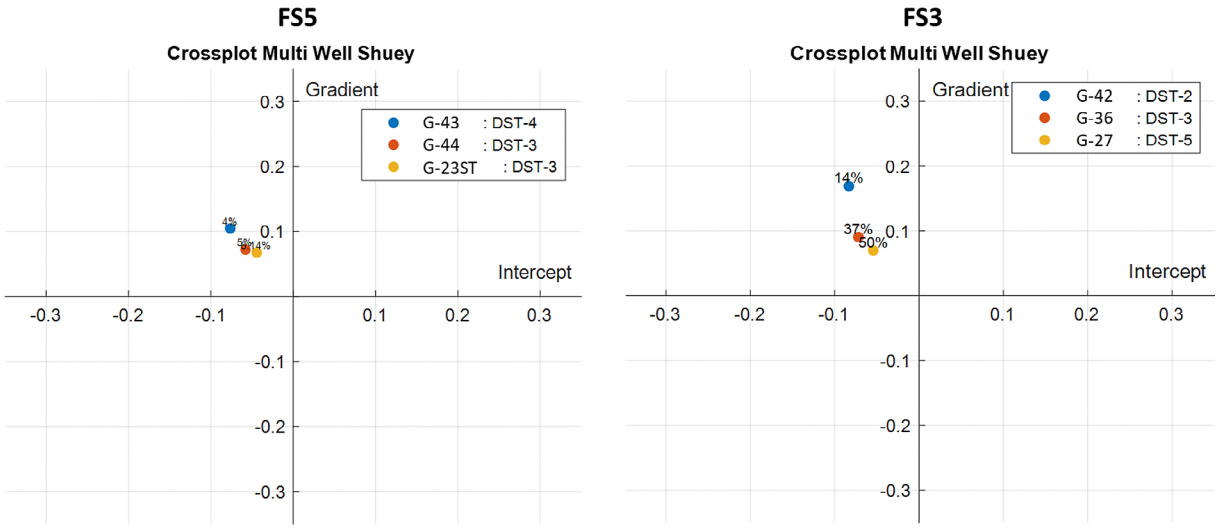

Well	DST	Intercept	Gradient	CO2 (%)
G-43	DST-4	-0.076452469	0.104449414	4
G-44	DST-3	-0.057900075	0.071938775	5
G-23ST	DST-3	-0.044211607	0.067352001	8.14

Well	DST	Intercept	Gradient	CO2 (%)
G-42	DST-2	-0.083190864	0.168794744	14
G-36	DST-3	-0.071832318	0.090241028	37
G-27	DST-5	-0.054286951	0.069710163	50

Figure 15: Crossplot of intercept and gradient attributes and their influence on changes in the percentage of CO_2 presence in the central compartment

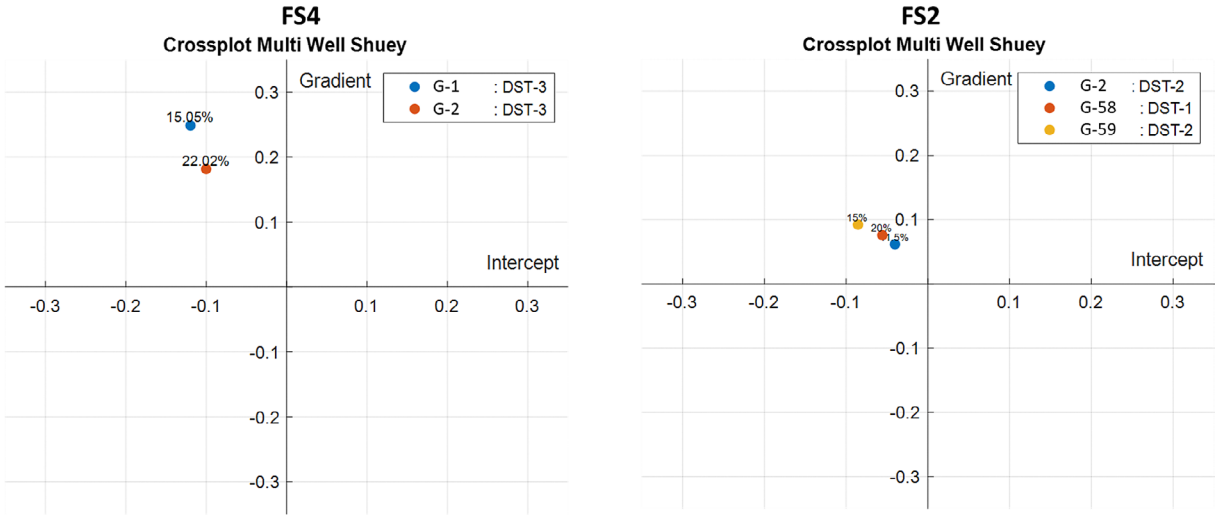

Well	DST	Intercept	Gradient	CO2 (%)
G-1	DST-3	-0.119598331	0.248607125	15.05
G-2	DST-3	-0.100081731	0.181599066	22.02

Well	DST	Intercept	Gradient	CO2 (%)
G-59	DST-2	-0.085492011	0.061819497	15
G-58	DST-1	-0.055723132	0.075995822	20
G-2	DST-2	-0.040265289	0.092459838	41.5

Figure 16: Crossplot of intercept and gradient attributes and their influence on changes in the percentage of CO2 presence in the southern compartment

ern sub-compartment 2, flooding surface 3 (FS3), wells G-17 and G-60 exhibit significantly different AVO classes (see **Figure 9**). This is supported by a crossplot between Poisson's ratio and P-impedance (see **Figure 17**). The crossplot reveals that the sample from well G-17 has a relatively large Poisson's ratio, aligning with the wet trend, indicating that its Poisson's ratio is nearly the same as the shale above it. In contrast, the Poisson's ratio of the sample from well G-60 is lower or almost identical to that of well G-17, and it falls within the wet trend, suggesting that this sample has fluid content dense enough, such as water. This indicates that the sample

Table 4: The summary of the intercept and gradient attributes for each FS interval and each compartment

Compartment	Interval	Well	DST	Depth	Depositional Environment	Facies	CO2 (%)	Intercept	Gradient	Etc.
North	FS6	G-46	DST#3	1898-1901	Transitional	Channel fill & Overbank mud	7	-0.1455	0.2490	Increase Intercept, Decrease Gradient
		G-19	DST#6	2121-2125			11.31	-0.0819	0.1154	
		G-20	DST#3	2044-2047			43.38	-0.0779	0.0850	
	FS4	G-18	DST#2	2056-2060	Meandering River	Channel fill & Overbank mud	11.26	-0.0935	0.1295	Increase Intercept, Decrease Gradient
		G-46	DST#2	1986-2003			19	-0.0581	0.0746	
		G-N1	DST#5	1849-1859			39.97	-0.0352	0.0497	
Middle	FS5	G-43	DST#4	1842-1846	Meandering River	Channel fill & Overbank mud	4	-0.0765	0.1045	Increase Intercept, Decrease Gradient
		G-44	DST#3	1998-2002			5	-0.0579	0.0719	
		G-23 ST	DST#3	2179-2188			8.14	-0.0442	0.0674	
	FS3	G-42	DST#2	2025-2026	Meandering River	Channel fill & Overbank mud	14	-0.0832	0.1688	Increase Intercept, Decrease Gradient
		G-36	DST#3	2112-2122			37	-0.0718	0.0902	
		G-27	DST#5	2057-2061			50	-0.0543	0.0697	
South	FS4	G-1	DST#3	1978-1982	Meandering River	Channel fill & Overbank mud	15.05	-0.1196	0.2486	Increase Intercept, Decrease Gradient
		G-2	DST#3	2094-2100			22.02	-0.1001	0.1816	
	FS2	G-59	DST#2	1944-1946	Braided-Meandering River	Channel fill & Overbank mud	15	-0.0855	0.0618	Increase Intercept, Decrease Gradient
		G-58	DST#1	2042-2046			20	-0.0557	0.0760	
		G-2	DST#2	2160-2166			41.5	-0.0403	0.0925	

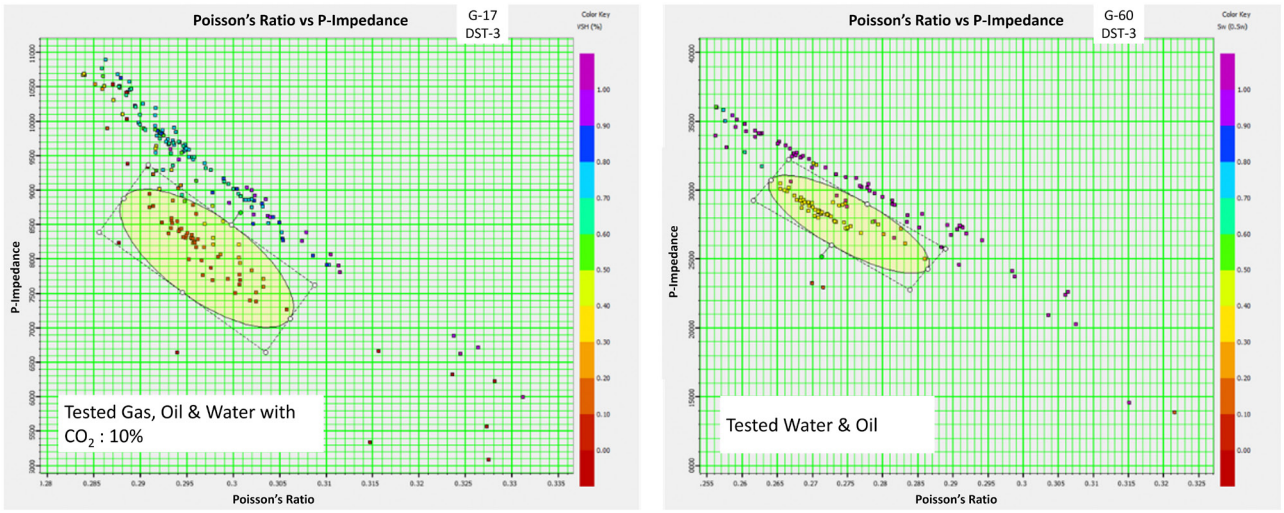

Figure 17: Crossplotting P-impedance with Poisson's ratio from wells G-17 and G-60

from well G-60 has a different AVO response, i.e., class 2 AVO. Therefore, based on this crossplot, a sample with CO_2 content will have a negative intercept and a positive gradient, in this case, representing class 4 AVO (well G-17), compared to a sample with water content showing a class 2 AVO response (well G-60).

Another example is in the southern compartment, southern sub-compartment 1, flooding surface 4 (FS4), where wells G-3, G-31, and G-1 exhibit different responses compared to the previous ones. Through the crossplot results, samples with CO2 content show class 4 AVO responses, indicated by a negative intercept and a positive gradient. For the sample from well G-3, the gas content is relatively high compared to the sample from well G-1. This is supported by a crossplot between poisson's ratio and p-impedance (see **Figure 18**). The crossplot reveals that samples from wells G-1 and G-31 have relatively large poisson's ratios, aligning with the wet

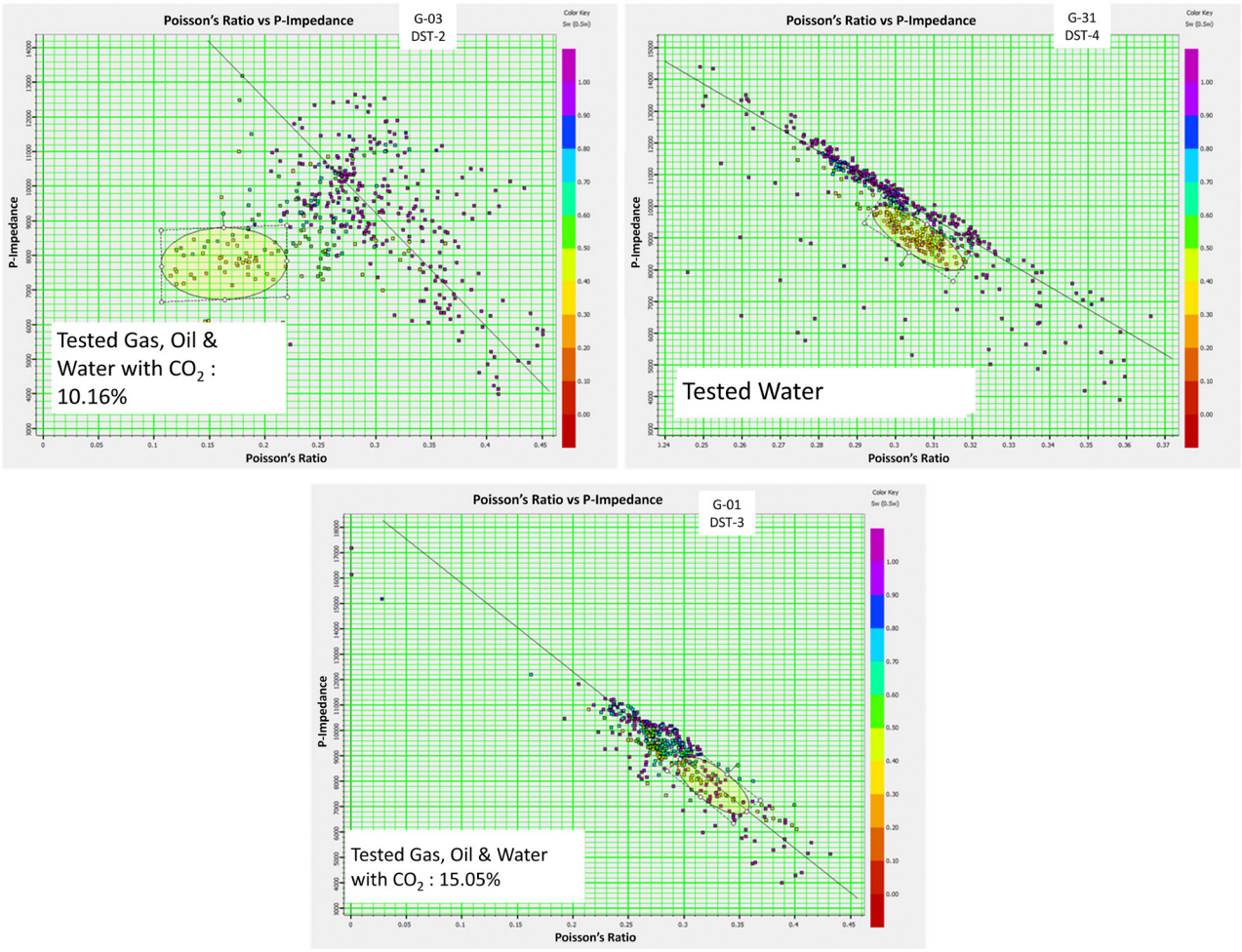

Figure 18: Crossplotting P-impedance with Poisson's ratio from wells G-3, G-31, and G-1

Table 5: The intercept and gradient respond to samples within the same depositional environment and varying depths

Depositional Environment	Well	DST	Depth	Interval	Facies	CO2 (%)	Intercept	Gradient	Etc.
Meandering River	G-43	DST#4	1842-1846	FS5	Channel fill & Overbank mud	4	-0.0765	0.1045	Increase Intercept, Decrease Gradient
	G-44	DST#3	1998-2002			5	-0.0579	0.0719	
	G-23 ST	DST#3	2179-2188			8.14	-0.0442	0.0674	
	G-1	DST#3	1978-1982	FS4	Channel fill & Overbank mud	15.05	-0.1196	0.2486	Increase Intercept, Decrease Gradient
	G-2	DST#3	2094-2100			22.02	-0.1001	0.1816	
Braided-Meandering River	G-28	DST#3	1959-1962	FS2	Channel fill & Overbank mud	40	-0.1259	0.1758	Increase Intercept, Decrease Gradient
	G-28	DST#2	1970-1975			45	-0.0587	0.0728	
	G-14	DST#2	2071-2076			50	-0.0373	0.0216	
	G-59	DST#2	1944-1946	FS2	Channel fill & Overbank mud	15	-0.0855	0.0618	Increase Intercept, Decrease Gradient
	G-58	DST#1	2042-2046			20	-0.0557	0.076	
	G-2	DST#2	2160-2166			41.5	-0.0403	0.0925	

trend, suggesting their poisson's ratio is nearly the same as the shale above them. In contrast, the poisson's ratio of the sample from well G-3 is lower and separated from the wet trend, indicating it is a soft sand with a high impedance shale interval above it. This results in the sample from well G-3 having a significantly different AVO response, i.e., class 3 AVO. Therefore, based on the representation of these three compartments, it can be concluded that the AVO response from CO_2 fluids is classified as class 4 AVO.

The classification of class 4 AVO for CO_2 fluids has been concluded in the previous analysis. Next is to ana-

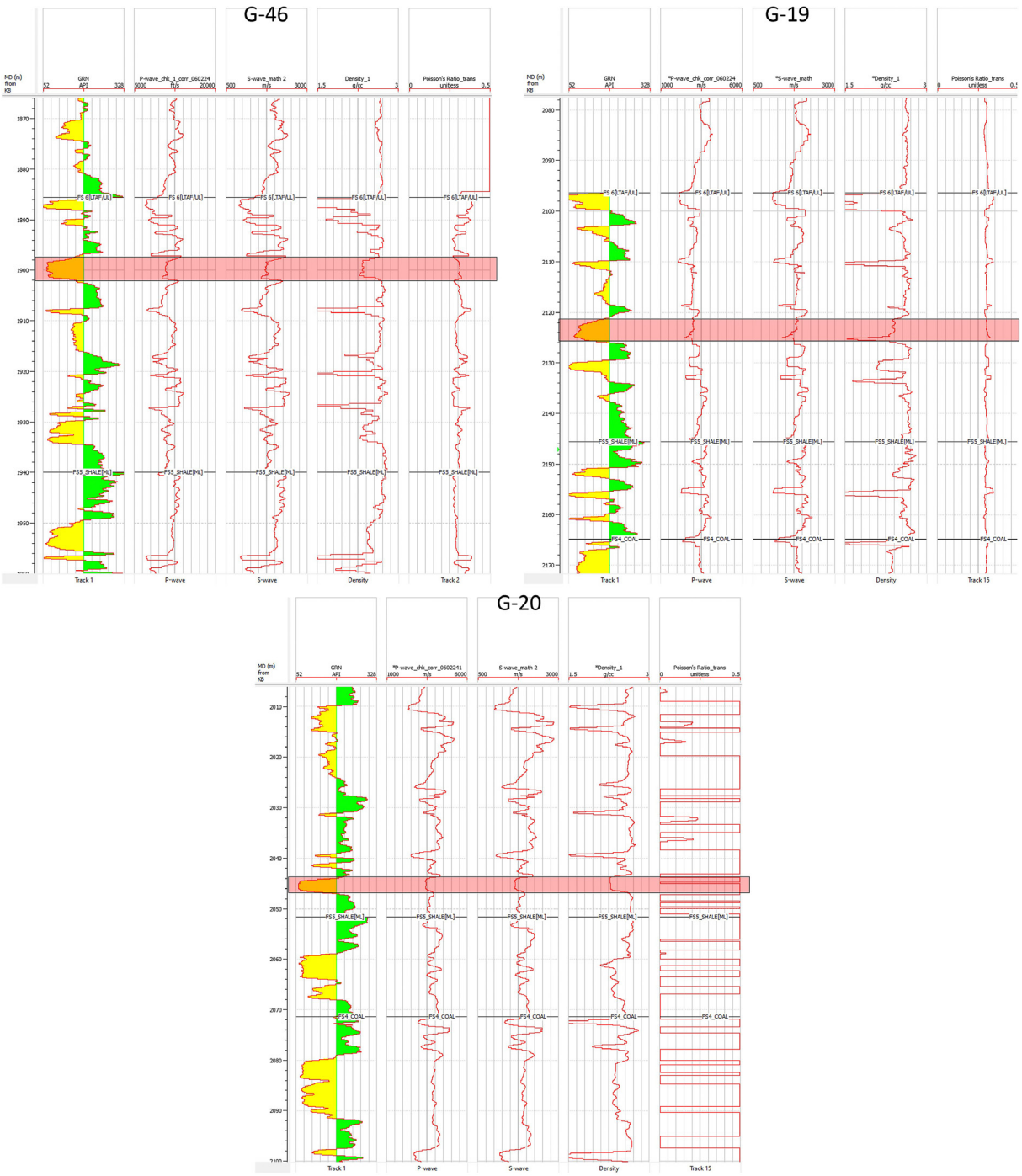

Figure 19: log response of the target interval for synthetic AVO gradient modelling on well G-46, G-19, and G-20

lyse the changes in AVO attribute responses, specifically intercept and gradient, with the variation in CO_2 saturation. The comparison results between the changes in CO_2 percentage and the crossplot of intercept and gradient attributes in the three compartments analysed in the previous section show a consistent trend in value changes. As the percentage of CO_2 increases, the intercept value becomes more positive, and the gradient value becomes more negative, or their changes tend towards class 2 AVO. To reinforce these findings, log responses were analyzed for the samples used in the analysis in subsection 3.3. It can be concluded that overall, in the interval of DST samples, the log responses of p-wave, s-wave, and density are smaller compared to the shale layers above them. These responses are associated with low Gamma-Ray values, indicating a sand lithology, as observed in samples from the northern compartment of FS6, such as G-46 DST-3, G-19 DST-6, and G-20 DST-3 (see **Figure 19)**. This can be further supported by lithological analysis, examining the relationship between Vp, porosity, and clay content, where the target interval is in the sand leg area and has low V-Shale values, indicating

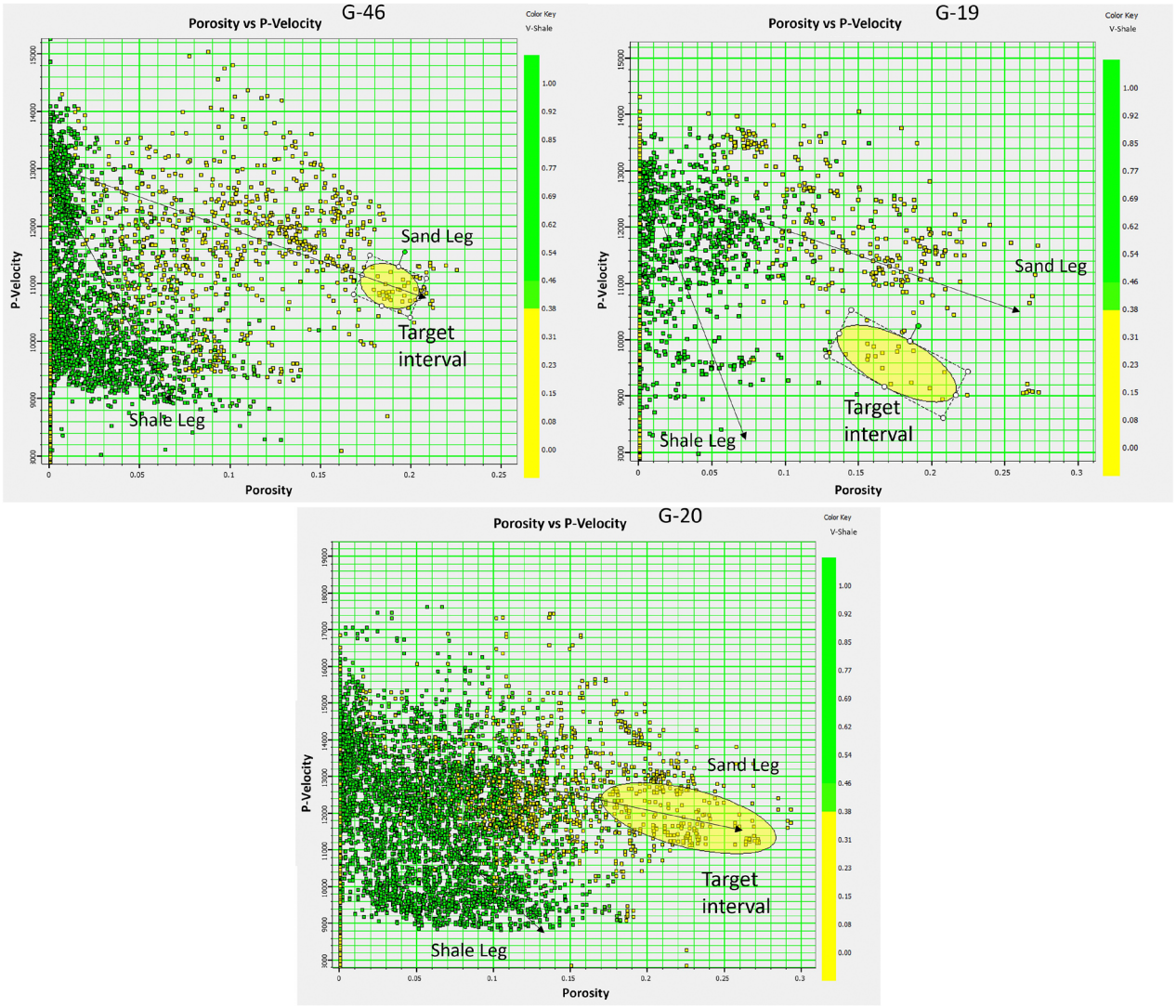

Figure 20: Lithology analysis using p-wave velocity, porosity and clay content parameter of the target interval for on well G-46, G-19, and G-20

Table 6: The intercept and gradient respond to samples within the same depth and varying depositional environments

Compartment	Depth	Depositional Environment	Well	DST	Facies	CO2 (%)	Intercept	Gradient	Etc.
North	2056-2060	Meandering River	G-18	DST#2	Channel fill & Overbank mud	11.26	-0.0935	0.1295	Increase Intercept, Decrease Gradient
North	2044-2047	Transitional	G-20	DST#3		43.38	-0.0779	0.085	
South	2071-2076	Braided-Meandering River	G-14	DST#2		50	-0.0373	0.0216	

a sand lithology (Sand ≤ 0.38, Shale > 0.38), as observed in samples from the northern compartment of FS6 (see **Figure 20)**.

This analysis also supported by the facies distribution obtained from the correlation of well facies in each sequence interval, where the northern compartment (**Figure 21**), central compartment (**Figure 22**), and southern compartment (**Figure 23**) all exhibit the same facies distribution, namely channel fill with overbank mud, indicating a fluvial deposition environment. From **Table 4**, it can be inferred that across all compartments and flooding surface (FS) intervals, samples with low to high CO_2 content consistently display AVO attribute responses characterized by an increase in intercept and a decrease

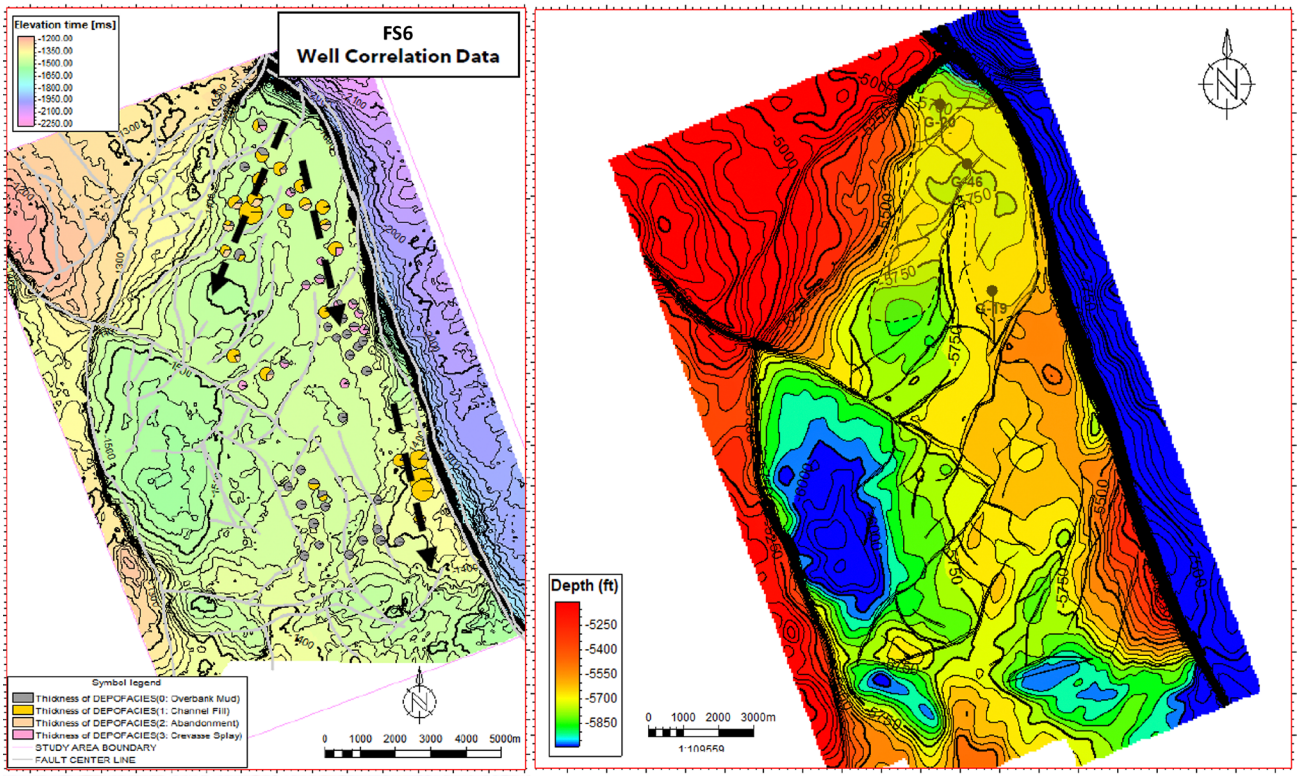

Figure 21: Map of facies distribution in the FS6 interval based on well facies correlation

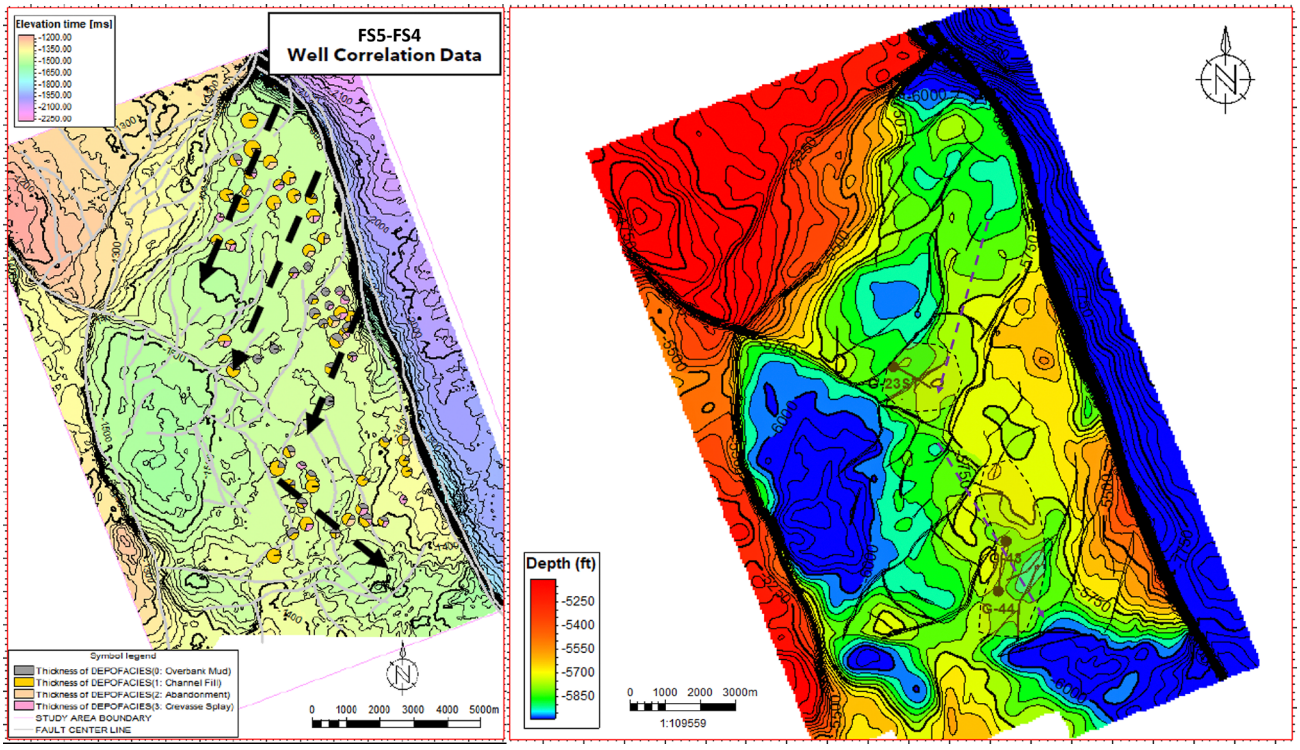

Figure 22: Map of facies distribution in the FS5-FS4 interval based on well facies correlation

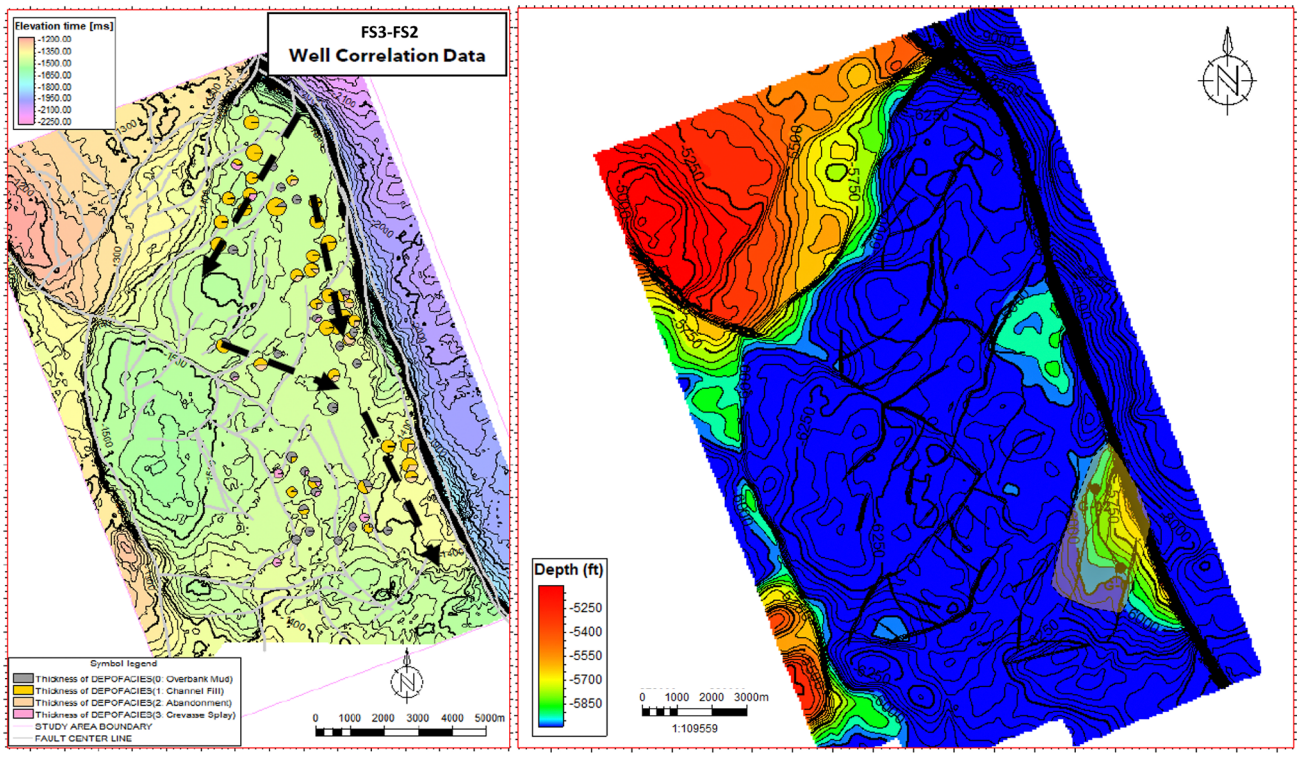

Figure 23: Map of facies distribution in the FS3-FS2 interval based on well facies correlation

in gradient, regredless of facies changes and depth changes, as observed in **Table 5** and **Table 6**. Therefore, in the research area, samples or areas with high CO_2 content will be classified as class 4 AVO, with intercept and gradient values approaching class 2 AVO.

5. Conclusions

Based on the analysis comparing the AVO responses between CO_2 and hydrocarbon fluids, the AVO classification obtained is class 4 AVO, supported by a higher Poisson's ratio that is nearly identical to the wet trend compared to other hydrocarbon fluids. The analysis of the influence of CO_2 presence on AVO attributes, particularly intercept and gradient, has been conducted using AVO modelling on well data. The results indicate that as the CO_2 percentage increases, the intercept value becomes more positive, and the gradient value becomes more negative, or their changes tend towards class 2 AVO. Therefore, AVO attributes, through well data AVO modelling, prove to be sufficiently sensitive in detecting the presence and changes in CO_2 percentage. The log responses further indicated that overall, the samples utilized in the analysis exhibit smaller log responses of p-wave, s-wave, and density within the interval of DST samples compared to the shale layers above them. These responses are correlated with low Gamma-Ray values, signifying a sand lithology. This inference can be reinforced through lithological analysis, which explores the relationship between Vp, porosity, and clay content. In this context, the target interval is situated in the sand leg region and demonstrates low V-Shale values, indicative of a sand lithology. In terms of facies and depth variations, the AVO attribute response consistently demonstrates an increase in intercept and a decrease in gradient with rising CO_2 levels.

Analysis of changes in CO_2 percentage in the research area using seismic data is highly recommended. In addition to comparing AVO responses from both well and seismic data, the distribution patterns of CO_2 with various saturations in the research area can be identified. However, the seismic data used must have adequate resolution to resolve thin layers in the Lower Talang Akar Formation.

Acknowledgment

The authors would like to express their gratitude to PetroChina International Jabung Ltd. for providing the data used in this research.

6. References

Alamsyah, M.N., Fitrianto, T., Sukmono, S., and Winardhi, S. (2023): A preliminary analysis of natural CO2-saturated gas sands distribution in the Gemah Field-Jabung Block, South Sumatra Basin, Indonesia, by using simple seismic attributes. The Leading Edge 42: 748–754. https://doi.org/10.1190/tle42110748.1

Aki, K., and Richards, P. G. (2002): Quantitative seismology. Mill Valley, California, 8 p.

Ambarsari, D. S., Sukmono, S., Winardhi, I. S., Sanny, T. A., Wardaya, P. D., Septama, E., Setiawan, T., Mulawarman,

A., Pratama, R. R., Rossa, V. I., and Murdianto, B. (2021): The effects of lithology and facies types on the anisotropy parameters and upscaling factor of the sand reservoirs in the deep-water Sadewa field, Kutei Basin, East Kalimantan, Indonesia. First Break, 39, 85–91. https://doi.org/10.3997/1365-2397.fb2021024

Anyosa, S., Bunting, S., Eidsvik, J., Romdhane, A., and Bergmo, P. (2021): Assessing the value of seismic monitoring of CO2 storage using simulations and statistical analysis. International Journal of Greenhouse Gas Control, 105, 1-5. https://doi.org/10.1016/j.ijggc.2020.103219

Castagna, J. P., Swan, H. W., and Foster, D. J. (1998): Framework for AVO gradient and intercept interpretation. Geophysics, 63, 948–956. https://doi.org/10.1190/1.1444406

Dupuy, B., Torres, V. A. C., Ghaderi, A., Querendez, E., & Mezyk, M. (2017): Constrained AVO for CO2 Storage Monitoring at Sleipner. In: 13th International Conference on Greenhouse Gas Control Technologies. – Elsevier Ltd., 3927–3936. https://doi.org/10.1016/j.egypro.2017.03.1524

Farfour, M., and Foster, D. J. (2021): New AVO expression and attribute based on scaled Poisson reflectivity. Journal of Applied Geophysics, 185, 1–8. https://doi.org/10.1016/j.jappgeo.2021.104255

Farfour, M., and Foster, D. (2022): Detection of hydrocarbon-saturated reservoirs in a challenging geological setting using AVO attributes: A case study from Poseidon field, Offshore Northwest region of Australia. Journal of Applied Geophysics, 203, 1–11. https://doi.org/10.1016/j.jappgeo.2022.104687

Farfour, M., Yoon, W. J., and Jang, S. H. (2016): Energy-weighted Amplitude Variation with Offset: A new AVO attribute for low impedance gas sands. Journal of Applied Geophysics, 129, 167–177. https://doi.org/10.1016/j.jappgeo.2016.03.032

Fatti, J. L., Smith, G. C., Vail, P. J., Strauss, P. J., and Levitt, P. R. (1994): Detection of gas in sandstone reservoirs using AVO analysis: A 3-D seismic case history using the Geostack technique. Geophysics, 59, 1362-1375.

Ginger, D., and Fielding, K. (2005): The Petroleum Systems and Future Potential of The South Sumatra Basin. In: Thirtieth Annual Convention & Exhibition. – IPA, 67–89, 68-75 p.

Ridwan, T. K., Hermana, M., Lubis, L. A., and Riyadi, Z. A. (2020): New avo attributes and their applications for facies and hydrocarbon prediction: A case study from the northern malay basin. Applied Sciences, 10, 1–17. https://doi.org/10.3390/app10217786

Sari, V. M., Sukmono, S., Sanny, T. A., and Sapiie, B. (2018): Seismic anisotropy estimation of the Talang Akar formation in south Sumatra basin, Indonesia, using ultrasonic tomography in core plugs. First Break, 36, 61–70. https://doi.org/10.3997/1365-2397.n0093

Setyaningsih, C. A., Lelono, E. B., & Firdaus, I. (2015): Palynological Study of the jambi Sub-Basin, South Sumatra. Scientific Contribution Oil and Gas, 38, 1-12.

Shuey, R. T. (1985): A simplification of the Zoeppritz equations. Geophysics, 50, 609–614.

Sukmono, S., Machado, V., Adelina, R., and Ambarsari, D. (2017): Integration of 3D seismic attributes for preliminary shallow geohazard identification in deep water exploration area with no well data. First Break, 35, 91–97. https://doi.org/10.3997/1365-2397.35.8.89810

Wiggins, R., Kenny, G. S., and McClure, C. D. (1983): A Method for Determining and Displaying the Shear-Velocity Reflectivities of a Geologic Formation. (0113 944). European Patent Application.

SAŽETAK

Utvrđivanje utjecaja prisutnosti CO_2 na odnos amplitude i pomaka u formaciji Lower Talang Akar, bazen Južne Sumatre, korištenjem metode modeliranja odnosa amplitude i pomaka

Područje je istraživanja naftno i plinsko polje u južnome bazenu Sumatre, koje je trenutno u fazi razvoja. Na ovome polju česte su pojave ugljena, posebice u formaciji Lower Talang Akar (LTAF), pri čemu spomenuti sadržaj ugljena predstavlja *in situ* izvor CO_2. Sadržaj CO_2 može se utvrditi pomoću metode analize odnosa amplitude i pomaka (engl. *Amplitude Versus Offset analysis*, AVO), što omogućuje procjenu utjecaja postotka CO_2 na navedeni odnos. Podatci korišteni u ovome radu uzimaju u obzir podatke o bušotinama, uključujući karotažne podatke (gustoća, poroznost, Vp & Vs Sonic/DT), podatke ispitivanja bušotine (engl. *Drill Stem Test*, DST), podatke markera bušotine, koji proizlaze iz interpretacije stratigrafske sekvencije i izvješća o bušotinama. Korištena AVO metoda obuhvaća širokokutni raspon, približno o° – 45°. Rezultati dobiveni ovim istraživanjem pomoću AVO metode, nakon AVO modeliranja na podatcima iz bušotine, pokazuju da je dominantan AVO odgovor, unutar LTAF intervala, klasa 4 AVO-a. Rezultati analize AVO-a, u vezi s prisutnošću AVO-a, pokazuju da intervali ležišta koji sadržavaju CO_2 imaju AVO odgovor klase 4 te da povećanje udjela fluida rezultira presijecanjima u pozitivnim vrijednostima i negativnijim gradijentom (prema klasi 2 AVO-a). Što se tiče facijesa i varijacija dubine, AVO odgovor dosljedno pokazuje povećanje presjeka i smanjenje gradijenta s porastom udjela CO_2.

Ključne riječi:
formacija Lower Talang Akar, udio CO_2, AVO analiza, AVO modeliranje, gradijent

Author's contribution

Muhammad Reza Perdana (1) (B.Eng., Geophysical Engineering with expertise in Seismic Exploration) provided the data analysis and interpretation and composed the original draft and editing. **Muhammad Noor Alamsyah (2)** (M.Sc., Geophysical Engineering with expertise in Seismic Interretation and Reservoir Characterization) provided the data interpretation, editing draft, supervision, and data collection. **Sigit Sukmono (3)** (Ph.D., Professor, expert on Petroleum Geophysics) provided the data interpretation on geophysical analysis, editing draft, and supervision. **Andri Hendriyana (4)** (Dr., Assistant Professor, Geophysical Engineering with expertise in Seismic Processing and Imaging) provide the data analysis and supervision.